NOTE TO USERS

This reproduction is the best copy available.

 $UMI^{^{\bullet}}$

Coupled Simulation of an Indirect Field Oriented Controlled Induction Motor Drive

Michael Legesse, B. Eng

Computational Analysis and Design Laboratory

Department of Electrical Engineering

McGill University, Montreal, Canada



A Thesis submitted to the Faculty of Graduate Studies and Research
In partial fulfillment of the requirements for the degree of
Master of Engineering

September 2008

© 2008 Michael Legesse



Library and Archives Canada

Published Heritage Branch

395 Wellington Street Ottawa ON K1A 0N4 Canada Bibliothèque et Archives Canada

Direction du Patrimoine de l'édition

395, rue Wellington Ottawa ON K1A 0N4 Canada

> Your file Votre référence ISBN: 978-0-494-66950-1 Our file Notre référence ISBN: 978-0-494-66950-1

NOTICE:

The author has granted a non-exclusive license allowing Library and Archives Canada to reproduce, publish, archive, preserve, conserve, communicate to the public by telecommunication or on the Internet, loan, distribute and sell theses worldwide, for commercial or non-commercial purposes, in microform, paper, electronic and/or any other formats.

The author retains copyright ownership and moral rights in this thesis. Neither the thesis nor substantial extracts from it may be printed or otherwise reproduced without the author's permission.

AVIS:

L'auteur a accordé une licence non exclusive permettant à la Bibliothèque et Archives Canada de reproduire, publier, archiver, sauvegarder, conserver, transmettre au public par télécommunication ou par l'Internet, prêter, distribuer et vendre des thèses partout dans le monde, à des fins commerciales ou autres, sur support microforme, papier, électronique et/ou autres formats.

L'auteur conserve la propriété du droit d'auteur et des droits moraux qui protège cette thèse. Ni la thèse ni des extraits substantiels de celle-ci ne doivent être imprimés ou autrement reproduits sans son autorisation.

In compliance with the Canadian Privacy Act some supporting forms may have been removed from this thesis.

While these forms may be included in the document page count, their removal does not represent any loss of content from the thesis.

Conformément à la loi canadienne sur la protection de la vie privée, quelques formulaires secondaires ont été enlevés de cette thèse.

Bien que ces formulaires aient inclus dans la pagination, il n'y aura aucun contenu manquant.



Abstract

Conventionally, system simulations of induction motor drives use lumped parameters model of the motor. This approach assumes motor parameters to be constant during the entire operation of the drive. Unfortunately, these are known to vary significantly over the operating range of the motor due to factors such as magnetic saturation, skin effects, and operating temperature. The variations in motor parameters affect motor output and control parameters resulting in degraded drive performance. One way of overcoming this problem is by coupling the field model of the induction motor with the drive simulation. By replacing the lumped parameters model with the field model, the influence of different operating conditions on motor parameters can be taken into account dynamically. In this thesis such an approach is investigated by coupling the finite element analysis of an induction motor with the system simulation of the field oriented controlled drive. The results obtained for the coupled simulation are promising and possible future works to make this method of simulation more accurate and reliable are recommended.

Résumé

Les simulations conventionnelles des moteurs à induction utilisent les paramètres localisés pour la modélisation du moteur. L'utilisation des paramètres localisés assume que les caractéristiques physiques du moteur ne changent pas pendant l'opération du moteur. Malheureusement, les caractéristiques physiques du moteur change de manière significative pendant l'opération du moteur à cause de la saturation magnétique, les effets de peau, et la température. Les variations de paramètres du moteur affectent la performance du moteur. Une façon de surmonter ce problème est par l'accouplement d'une modèle électromagnétique du moteur à induction avec le simulateur. Dans cette thèse, les paramètres localisés dans le model du moteur sont remplacés par une modèle électromagnétique utilisant la méthode des éléments finis. Les résultats obtenus pour l'accouplement de simulation démontrent que cette méthode est fiable. Des méthodes de simulation plus précises et fiables sont recommandées.

Acknowledgements

I would like to express my sincere thanks to Professor David Alister Lowther, my thesis advisor, for his continuous support and guidance throughout my entire Masters study at McGill University. His valuable suggestion and encouragement were important for the completion of this thesis.

I would also like to thank all my friends at Computer Aided Design Laboratory for their collaborations and friendship during my study period at McGill. Thanks also goes to Adrian Ngoly for helping me translate the abstract of this thesis to French.

Finally, I would like to express my special gratitude to my family - my mother, my brother and his wife, and my two sisters for all the help they have given me over the years – Thank you.

Table of Contents

A	bstr	act		2
R	ésur	mé		3
Α	.ckn	owle	edgements	4
Т	able	of C	Contents	5
L	ist o	f Syn	mbols	7
L	ist o	f Figu	gures	9
		_	bles	
1			oduction	
_				
	1.1		Problem Description	
	1.2	<u>)</u>	Literature review	14
		1.2.1	1 Finite Element Analysis of Induction Machines	14
		1.2.2	2 Field Oriented Control of Induction Machines	16
		1.2.3	3 Coupled Simulation	17
	1.3	3 (Outline of the Thesis	19
2	ı	Finite	te Element Analysis of Induction Motors	20
	2.1	L I	Review of equations of electromagnetics	20
	2.2	2	Finite element analysis	22
	;	2.2.1	1 Electromagnetic field formulation	23
	;	2.2.2	2 Force/torque calculation	26
	2.3	3	Modeling and analysis of an induction motor using MagNet	28
	;	2.3.1	1 Modeling the induction machine	30
	:	2.3.2	2 Simulation of the no-load test	39
	;	2.3.3	3 Simulation of the locked-rotor test	41
	:	2.3.4	4 Transient field analysis	46
3	İ	Field	d Oriented Control of Induction Motors	48
	3.1		Two-axes representation of the induction motor	48

	3.2	Prin	ciple of field orientation	52
	3.3	Desc	cription of the FOC drive system	54
	3.3.	1	Speed controller	56
	3.3.	2	Flux/Torque calculator	56
	3.3.	3	Flux/Torque controller	58
	3.4	Simi	ulation results	60
4	Cou	pled :	Simulation	65
	4.1	Cou	pling methods	66
	4.1.	1	Direct coupling	66
	4.1.	2	Indirect coupling	69
	4.2	Impl	lementation	71
	4.3	Simi	ulation results and discussion	74
5	Con	clusic	on and Future Work	79
	5.1	Futu	re work	79
	5.1.	1	Integration of thermal effects	79
	5.1.	2	Comparison with measured results	80
	5.1.	3	Response surface methodology	81
	5.2	Sum	mary	82
Rε	ferenc	es		84
Αŗ	pendix	κ A		88
	No-loa	d sim	rulation result	88
	Locked	d-roto	or simulation result	89
Αŗ	pendix	к В		90
	The Fir	nite F	lement Method	90

List of Symbols

Boldface symbols are used for vectors.

Н	magnetic field strength
J	current density
D	electric flux density
E	electric field strength
В	magnetic flux density
v	velocity of conductor
ρ	electric charge density
ϵ	permittivity of material
μ	magnetic permeability of material
σ	conductivity of material
Α	magnetic vector potential
V	voltage applied to conductors of a field region
I	current flowing in the conductors of a field region
ν	magnetic reluctivity
R_s	stator inductance
L_{ls}	leakage inductance
R_r	rotor resistance
L_{lr}	rotor leakage inductance
L_m	magnetizing inductance
W_m	total stored magnetic energy
I_{srms}	RMS stator current

v_s	stator voltage
v_r	rotor voltage
i_s	stator current
i_r	rotor current
λ_s	stator flux linkage
λ_r	rotor flux linkage
T_L	external torque
T_e	electromagnetic torque
P_r	rotor power losses
P	number of pole pairs
R_{eq}	equivalent rotor resistance
L_{eq}	equivalent rotor inductance
J	moment of inertia
ω_r	angular velocity/mechanical speed of the rotor
$ heta_f$	rotor flux angle
$ heta_r$	rotor position
$ heta_{sl}$	slip angle
ω_{sl}	angular slip frequency
$ au_r$	rotor time constant

List of Figures

Figure 2-1 Equivalent circuit of cage induction motor	29
Figure 2-2 Cross-section of the induction motor	31
Figure 2-3 Virtual Air Shield Method	33
Figure 2-4 Quarter model of the induction motor	34
Figure 2-5 Stator winding circuit	
Figure 2-6 Meshed model of the induction motor	38
Figure 2-7 Flux plot under no-load condition	
Figure 2-8 Flux-linkage versus stator current	40
Figure 2-9 Magnetizing inductance vs. current	40
Figure 2-10 Locked-rotor flux-plot for 50 Hz	42
Figure 2-11 Locked-rotor flux-plot for 10 Hz	43
Figure 2-12 Torque vs. slip	44
Figure 2-13 Equivalent circuits corresponding to the locked-rotor simulation	45
Figure 2-14 Electromagnetic torque vs. time	
Figure 2-15 Mechanical speed vs. time	47
Figure 3-1 Equivalent circuit of the dq-axes model of the induction motor	51
Figure 3-2 Rotor flux field orientation	53
Figure 3-3 Overview of FOC drive system [39]	55
Figure 3-4 Speed - PI controller	56
Figure 3-5 Rotor flux angle calculation block	57
Figure 3-6 ABC - dq axes transformation	58
Figure 3-7 Hysteresis-band PWM	59
Figure 3-8 Simulink implementation of the Current regulator	60
Figure 3-9 Waveforms of speed, current, and torque at start-up	62
Figure 3-10 Waveforms of speed, current, and torque during load change	63

Figure 4-1 A block diagram of indirect coupling using sources	70
Figure 4-2 A block diagram of indirect coupling using <i>Ldyn</i> and <i>e</i>	71
Figure 4-3 MagNet-Simulink Plug-in and its pins	73
Figure 4-4 Schematic of the coupled simulation	74
Figure 4-5 Coupled simulation waveforms of speed, current, and torque at start-up	76
Figure 4-6 Coupled simulation waveforms of speed, current, and torque during load change 7	77

List of Tables

Table 2.1 Motor Rating	. 29
Table 2.2 Motor data	. 31
Table 3.1 Lumped parameters of the induction motor	. 61

1 Introduction

In the environmentally conscious world in which we are living today the efficient production and use of electrical energy is a major issue. In the last three decades, this concern for the environment coupled with the ever increasing cost of energy has encouraged the development of highly advanced and sophisticated energy conversion systems [1; 2]. Alongside these developments, the design and analysis tools used by engineers for modeling and simulating the electrical machines, power converters, and control systems that make up the energy conversion systems have seen significant improvements.

The finite element method (FEM) is one such tool that is widely used in the design and analysis of electrical machines. The developments of solution methods and advancements in computational hardware over the years have made this numerical field analysis method very attractive for researchers and designers alike. Particularly, its ability to take into account irregular geometric shapes of components makes it well suited to carry out electromagnetic field analysis of electrical machines.

Power converters, on the other hand, can be modeled by one of several excellent circuit simulators that are now available. These software tools include but are not limited to - PSPICE, PSIM, and PSCAD. But when it comes to modeling converters as part of a drive system, it is preferred to model them with their control system using system simulators. In this regard, by far the most common system simulation environment in the industry is Simulink.

Although the tools mentioned thus far are excellent in their specialized field, there are not that many tools currently available which combine the best features of, for example, FEM and Simulink, in one single environment. The design of high performance energy conversion systems will surely benefit from such modeling and simulation packages as they will provide the designer with the ability to model electrical machines, power converters, and control systems accurately in a single environment facilitating the design process.

1.1 Problem Description

Traditionally, the design of converters and electrical machines has been carried out separately. But manufacturers are looking more and more to a combined design process to increase efficiency and performance and to lower production costs. Particularly in large electric drives, both the electrical machine and the power converter are tailored to work together to guarantee the best possible performance for the application. In cases like this, a combined simulation environment, where the electromagnetic field analysis of the electrical machine is coupled with a detailed model of the converter and the control system is very useful. In this thesis such a simulation environment is presented and used in modeling and analysis of a vector controlled induction motor drive system. This modeling and simulation tool is implemented by coupling *MagNet*, a commercial field analysis package, with *Simulink*, a system simulator.

1.2 Literature review

This section reviews previous work done in the three main areas of this thesis, which are – the finite element analysis of an induction machine, field oriented control of induction machines, and the coupled simulation of finite element analysis of electrical machines with power converters and closed loop control systems.

1.2.1 Finite Element Analysis of Induction Machines

The application of the finite element method for analyzing the magnetic fields of electrical machines was first reported in the literature in the late 1960's. Chari and Silvester applied the FEM in the analysis of synchronous machines [3] and DC-machines [4]. These machines were chosen at the time because their operation can be approximately modeled by stationary fields. It would be another decade before FEM was applied for the analysis of electrical machines, such as the induction motor, whose field is time dependent.

Among the first publications to deal with the use of FEM in the analysis of induction machines is the paper by Ito et al. [5]. In this work, the magnetic field distribution in a three-phase squirrel-cage induction motor is computed using a two-dimensional field formulation and assuming sinusoidal time variation. Williamson and Ralph [6] modeled a single-phase induction motor with a constant voltage source, assuming uniformly distributed sinusoidal currents in the stator and rotor coils. The finite element analysis for this induction machine included the effects of

rotor harmonics and rotor skew. Williamson and Bebb [7] extended this model by including eddy currents in the formulation. The paper outlines a general method for combining circuit and field analysis for the purpose of predicting the performance of cage induction motor.

A time-stepping methodology for solving magnetic field problems is presented by MacBain in [8]. In this paper, the non-linear diffusion equation that describes the two-dimensional time-dependent magnetic field is solved with the FEM utilizing time-stepping techniques. This time-stepping approach is applied to an induction motor in [9] to analyze harmonic contents in the rotor bars and the magnetic permeability variation in the stator teeth throughout a time cycle. Arkkio described in [10] the finite element analysis of cage induction motors fed from static frequency converters. The non-sinusoidal voltage supplied from the Pulse Width Modulated (PWM) inverter is imposed on the stator windings of the machine and the resulting time-dependent field is modeled by the Crank-Nicholson time-stepping method.

The FEM is also used to identify electrical machine parameters. Williamson and Robinson used it in conjunction with the conventional equivalent circuit model in [11] to determine the equivalent circuit parameters of a three-phase cage induction motor. Escarela-Perez and MacDonald calculated the two axes transient parameters of a solid rotor turbine-generator using the FEM in [12]. Mohammed et al. in [13] developed a phase variable model of a brushless DC motor based on the inductances, back electromotive force, and the cogging torque obtained from non-linear transient finite element analysis of the machine.

As can be observed from the above works, the finite element analysis of the electromagnetic field within induction machines has matured over the years. Current researches in this area focus on coupling this analysis with analyses of other physical fields and external circuits that interact with the electromagnetic field in the machine. This thesis is undertaken in light of this current research direction.

1.2.2 Field Oriented Control of Induction Machines

The concept of field orientation was first proposed by Hasse [14] and Blaschke [15]. In both cases, the flux vector used for field orientation is the flux vector. Hasse suggests a field orientation scheme in which the rotor flux vector is acquired indirectly from measured rotor speed and calculated slip speed. In contrast, in Blaschke's implementation, the flux vector is directly measured using Hall probes, search coils, or other measurement techniques. These works were followed by a publication from Gabriel and Leonard [16], in which the authors describe the implementation of the field oriented control technique for an inverter-fed induction motor.

The performance of an indirect field oriented controlled induction drive system is highly dependent on the rotor time constant. Since this quantity varies during motor operation due to saturation, temperature, etc. parameter mismatch occurs between the motor model used to design the control system and the actual motor resulting in control performance degradation. In order to overcome this problem, a number of methods have been proposed to identify the

rotor time constant of an induction motor in an on-line process. Matuso and Lipo present in [17] an on-line rotor parameter identification technique for the purpose of updating the control gains of an induction motor vector controller. This identification technique involves injecting a negative sequence current and detecting the negative sequence voltage. The rotor resistance is then calculated from the obtained information. Other works reported in this area include [18; 19; 20].

This thesis investigates another method for taking into account motor parameter variations in the design and analysis of a Field Oriented Controlled induction motor drive system. The approach considered couples the transient field analysis of the induction machine with the system simulation of the power electronic and control circuits of the drive system.

1.2.3 Coupled Simulation

The application of numerical methods for solving field equations coupled with the circuit equations of the supply system is widely reported in the literature. Piriou and Razek in [21] investigate a two-dimensional saturated electromagnetic system associated with a non-linear electric circuit. The non-linear equations of the electric circuit are directly coupled with the field equations and the Newton-Raphson method is used to solve the resulting matrix system. Smith et al. describe a time-stepping finite-element technique for modeling transient torques and currents in a slip-ring induction motor in [22]. The method they used is based on a coupled field-circuit equation approach that allows the winding inductances to be modified to account

for certain three-dimensional effects. Other works that deal with the coupled field-circuit problem include [23; 24; 25; 26].

The inclusion of a closed loop control system within the field-circuit model has also attracted considerable interest. Demenko [27] used direct field-circuit coupling to simulate a permanent magnet motor drive with a simple control strategy, where the speed and position of the rotor were used for controlling the switches after each time step. Ito et al. [28] simulated a similar system by coupling the field analysis indirectly with the circuit and mechanical equations. Ho et al. [29] modeled a current hysteresis controller with a brushless DC motor drive in a similar manner, but an adaptive time-step control was added in order to keep the current within the hysteresis limit. A similar approach was also applied by Jabbar et al. [30] to a spindle motor drive with a current hysteresis controller. Kuo-Peng et al. [31] included the closed-loop control systems into the software for coupled field-circuit simulation, and applied the method to a nonlinear coil and transistor inverter with a current hysteresis controller. As a continuation, Roel Ortiz et al. [32] presented an approach in which the control signals for the switches are generated during the simulation and the time steps are automatically adjusted according to the control. The method was applied to a saturable inductor and a full bridge inverter with sliding mode control. Manot et al. [33] presented an application of the method to model an induction heating device supplied by a resonant converter. Kanerva et al. [34] presented a compound drive simulator, in which a finite element method model of an asynchronous machine is coupled with a frequency converter controlled by a direct torque control scheme.

This thesis continues to build on the above works reported in the area of coupling the finite element analysis of electromagnetic devices with the analysis of the external circuits and control systems associated with these devices.

1.3 Outline of the Thesis

The remainder of this thesis is organized as follows. Chapter 2 reviews the finite element analysis of induction motors and discusses the modeling and analysis of one such motor using commercial field analysis software. In Chapter 3, the theory of field oriented control is briefly reviewed and a description of a vector controlled induction motor drive system along with the Simulink implementation is presented. In Chapter 4, methods for coupling the finite element analysis of electrical machines with the circuit and control simulation are discussed and a coupled simulation environment is implemented for a vector controlled induction drive system. Finally, the conclusion of the thesis is presented in Chapter 5 and future work in the area is suggested.

2 Finite Element Analysis of Induction Motors

This chapter starts by giving a brief review of the fundamental equations of electromagnetics. The next section discusses the finite element analysis of induction motors. The last section is devoted to the modeling and analysis of a cage induction motor using a commercial field analysis software.

2.1 Review of equations of electromagnetics

Electromagnetic field analysis can be represented as the problem of solving Maxwell's equations subjected to certain boundary conditions. These equations state the relationships between the fundamental electromagnetic field quantities as follows —

$$\nabla \times \mathbf{H} = \mathbf{J} + \frac{\partial \mathbf{D}}{\partial t}$$
 (2.1)

$$\nabla \times \mathbf{E} = -\frac{\partial \mathbf{B}}{\partial t} + \nabla \times (\mathbf{v} \times \mathbf{B})$$
 (2.2)

$$\nabla \cdot \mathbf{D} = \rho \tag{2.3}$$

$$\nabla \cdot \mathbf{B} = 0 \tag{2.4}$$

where

- E, D are electric field intensity and electric flux density respectively
- H, B are the magnetic field intensity and magnetic flux density, respectively,
- J is the current density, and
- v is the velocity of the conductor with respect to **B**, and
- ρ is the electric charge density

In the analysis of electrical machines, the displacement current, $\partial \mathbf{D}/\partial t$, in equation (2.1), is disregarded since the frequencies of interest are usually low enough that the displacement current is negligible.

In addition to the Maxwell's equations, there are constitutive relations, which describe the properties of the material over which the electromagnetic field is to be solved. These relations are,

$$\mathbf{D} = \epsilon \mathbf{E} \tag{2.5}$$

$$\mathbf{B} = \mu \mathbf{H} \tag{2.6}$$

$$\mathbf{J} = \sigma \mathbf{E} \tag{2.7}$$

where ϵ is the permittivity of the material, μ is the magnetic permeability of the material , and σ - is the conductivity of the material

2.2 Finite element analysis

Traditionally, the design of induction motors has been done based on approximate knowledge of the electromagnetic field within the motor. In this approach, the dimensioning of the iron core and the evaluation of the motor performance are based on rough estimations of the field distribution in the motor. This method usually gives reasonable results for steady-state operation near the synchronous speed of the machine, but for the locked-rotor and transient operations the results are not reliable. In addition, since the classical analytical approach assumes the induction motor to be supplied from sinusoidal sources, it cannot be directly applied to the analysis of induction motors that are supplied by power converters.

More reliable calculation methods are required especially in the design of large and non-standard induction motors, as it is very expensive to construct prototypes to test the validity of a design. It is also important to be able to predict accurately the transient performance of high power induction motors, e.g. during start-up, in order to determine the requirements that will be imposed on the power supply.

The above limitations of the traditional method of design can be overcome by solving the field distribution in the machine from the Maxwell's equations.

2.2.1 Electromagnetic field formulation

Although the computational domains over which the electromagnetic field equations need to be solved are essentially three-dimensional, in cases such as electrical machines, where the stack length is sufficiently long, it is computationally less expensive to perform a two-dimensional field analysis. This kind of treatment is possible for devices which exhibit translational or rotational geometric symmetry, and the same type of symmetry with respect to the excitations, materials, and boundary conditions. Since the induction motor is translationally symmetric and its windings and excitations repeat every pole-pitch, a two-dimensional formulation can be employed for its analysis.

The two-dimensional field formulation is based on the magnetic vector potential, \mathbf{A} . Since the divergence of \mathbf{B} is zero (equation (2.4)), the magnetic vector potential can be related to the magnetic flux density as follows,

$$\mathbf{B} = \nabla \times \mathbf{A} \quad (2.8)$$

The magnetic vector potential is valuable when solving two-dimensional problems, because a current in, say, the z direction produces A_z only, and x and y components of \mathbf{B} . This simplifies equation (2.8) to.

$$\begin{cases} B_x = \frac{\partial A_z}{\partial y} \\ B_y = \frac{-\partial A_z}{\partial x} \end{cases}$$
 (2.9)

Substituting equation (2.8) into equations (2.2) and (2.6) results in,

$$\mathbf{E} = -\nabla V - \frac{\partial \mathbf{A}}{\partial t} + \boldsymbol{v} \times \nabla \times \mathbf{A}$$
 (2.10)

where ∇V is known from the specified voltage sources

and,

$$\mathbf{H} = \nu \nabla \times \mathbf{A} \tag{2.11}$$

where $v = \frac{1}{\mu}$ is the magnetic reluctivity.

Using the quasi-static approximation (i.e. equating $\partial \mathbf{D}/\partial t$ to zero) and substituting equations (2.7), (2.10), and (2.11) in (2.1) gives the following governing differential equation of the field problem,

$$\nabla \times \nu \nabla \times \mathbf{A} = \sigma \nabla V - \sigma \frac{\partial \mathbf{A}}{\partial t} + \sigma (\mathbf{v} \times \nabla \times \mathbf{A})$$
 (2.12)

The expression on the right side of the above equation represents the total current density, **J**. As it can be seen, **J** has three different parts; $\sigma \nabla V$, represent the current density due to the applied source, $\sigma \frac{\partial \mathbf{A}}{\partial t}$, the current density due to the induced electric field produced by timevarying magnetic flux, and $\mathbf{v} \times \nabla \times \mathbf{A}$, the motion-induced or speed voltage.

Equation (2.12) can be simplified to the form shown in equation (2.13) by employing a frame of reference that is fixed with respect to the motion component. As a result of this fixed reference frame the relative velocity, v, becomes zero.

$$\nabla \times \nu \nabla \times \mathbf{A} = \sigma \nabla V - \sigma \frac{\partial \mathbf{A}}{\partial t}$$
 (2.13)

Numerical methods available for solving equation (2.13) include the boundary element method, the finite difference method, and the finite element method. In this thesis, the numerical analysis is based on the finite element method owing to the fact that it is better at dealing with irregular geometries and non-linear materials than the other numerical methods.

In the two-dimensional finite element analysis of induction motors, the cross-section of the machine is discretized by dividing it into a mesh of elements. Then the field inside each element is approximated using a finite set of pre-determined basis functions with unknown coefficients. These functions are based on the nodes of the elements, with the requirement that the solution must be continuous across inter-element boundaries. The finite element analysis is the solution of the set of equations for these unknown coefficients. The finite element method is explained in detail in Appendix A.

There are several commercial finite element analysis software tools available on the market that can be used for electromagnetic field analysis of electrical machines. In this thesis *MagNet*, which is an electromagnetic simulation software from Infolytica[35], is used to carry out the field analysis of a squirrel-cage induction motor. This software package uses the finite element

method to solve low frequency magnetic boundary value problems, in which currents can be induced by time-varying and/or motional effects. Once the model is fully defined, *MagNet* solves Maxwell's equations to find the magnetic field within the model. The solvers available in the package can tackle all low frequency problems related to electrical machines, actuators, solenoids, transformers, and sensors.

After the magnetic fields are computed, they can be viewed as shaded, arrow or contour plots. The field plots can also be viewed as field animations. In addition, *MagNet* automatically extracts from the field solution certain global parameters of interest (e.g. energy, torque, etc.), depending on the solution type.

2.2.2 Force/torque calculation

Besides determining the field distribution and local field quantities, the main aim of the finite element analysis of the induction motor, is to accurately calculate global quantities, such as force, torque, energy, and flux linkage. In this section, two popular methods used for calculating the magnetic forces/torques in electrical machines from the finite element results are briefly discussed.

2.2.2.1 Maxwell stress method

The force calculation method used by *MagNet* for electrical machines is based on the Maxwell stress tensor method. In this method, the global magnetic force is found by first computing the

local stresses at all points of a bounding surface and then summing them using a surface integral. If the total field surrounding the body is known, the force exerted on the body in terms of that field is expressed as,

$$F = \oint_{S} \frac{1}{2\mu_0} (B_n^2 - B_t^2) \, ds \cdot \vec{t} + \oint_{S} \frac{1}{\mu_0} B_n B_t \, ds \cdot \vec{n}$$
 (2.14)

where s is the surface enveloping the body under force, n and t are unit vectors in the normal and tangential direction on the surface s, and μ_0 is the permeability of free space.

In two dimensional problems, the surface integral of the force density is reduced to a line integral, making the implementation of the Maxwell stress method relatively easy in these problems. However, the use of the above Maxwell stress formulae requires the integration path or surface to be closed, and situated entirely in a linear material. It is also known to be very susceptible to numerical errors, especially near sharp corners of electromagnetic devices, such as around the stator and rotor teeth of induction machines, where the field intensity is usually very high.

2.2.2.2 Virtual work method

The virtual work method for computing the electromagnetic force is derived from the magnetic stored energy, W_m (or co-energy, W_m') changes against space displacement. There are two implementations of this method. In the first implementation, the force on an object is found as the derivative of the magnetic energy with respect to position at constant flux linkages or the

derivative of magnetic co-energy with respect to position at constant current. In a case in which the co-energy is used this force is given as

$$F_{vw} = \frac{W_{2m}' - W_{1m}'}{\Lambda s} \tag{2.15}$$

where W'_{1m} and W'_{2m} are co-energies evaluated at two successive positions and Δs is the displacement between the two positions.

The second implementation is what is referred to as the Coulomb's virtual work method. In this approach, the energy functional is directly differentiated with respect to a virtual displacement eliminating the need for two solutions.

2.3 Modeling and analysis of an induction motor using MagNet

The device considered in this thesis is a three phase, four-pole, star-connected squirrel-cage induction motor [36]. The ratings of the motor are given in Table 2.1. A two-dimensional model of the motor is constructed in *MagNet*, and a field analysis of the device is carried out using *MagNet's* static, time-harmonic, and transient with motion solvers. The static and time-harmonic solvers are used to simulate the no load test and the locked rotor test respectively. At no-load, magneto-static simulations are carried out by varying the magnetizing current. In the locked-rotor test, time-harmonic simulations are carried out at different rotor frequencies so as to compute the dependence of the rotor parameters on the slip frequency. From these two

tests, the parameters for the equivalent circuit of the induction motor (Figure 2-1) are obtained, from which the motor performance is predicted and operation characteristics are calculated. Finally, *MagNet's* transient with motion solver is used to perform a time-stepping finite analysis of the motor taking into account the movement of the rotor.

Motor	Ratings
rated power	5.5 kW
rated voltage	460 V
rated current	9 A
rated frequency	60 Hz

Table 2.1 Motor Rating

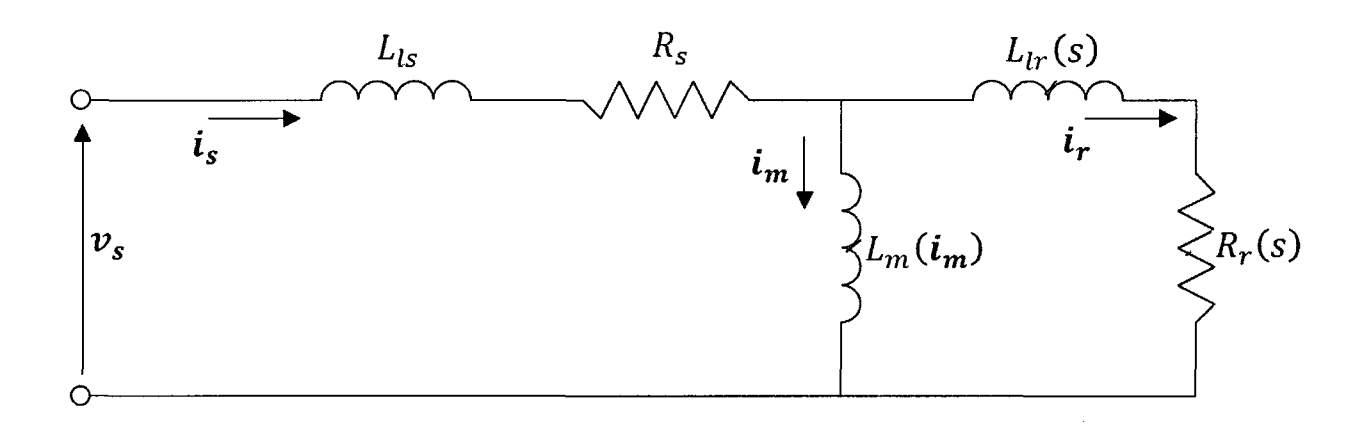


Figure 2-1 Equivalent circuit of cage induction motor

where

- R_s (Ω) is stator inductance,
- L_{ls} (H) is stator leakage inductance,
- R_r (Ω) is rotor resistance referred to the stator,
- L_{lr} (H) is rotor leakage inductance,
- L_m (H) is magnetizing inductance, and
- s is slip

2.3.1 Modeling the induction machine

This section discusses some of the issues involved in the modeling process of the induction machine in *MagNet*.

2.3.1.1 Geometric and material modeling

The first step in the modeling process is the construction of an air box that encompasses the induction motor completely to limit the extent of the computational domain. Then the cross-sections of the stator and rotor core are drawn in the *xy-plane* according to the geometrical details provided in Table 2.2. Finally, the whole model is extended in straight line in the *z-direction* to form the solid body and materials are assigned to different parts of the machine.

36	Stator slot pitch	9.7 mm
28	Rotor slot pitch	12.5 mm
190 mm	Air gap	0.35 mm
11.5 mm	Shaft diameter	35 mm
112 mm	Stack length	132 mm
	28 190 mm 11.5 mm	28 Rotor slot pitch 190 mm Air gap 11.5 mm Shaft diameter

Table 2.2 Motor data

The cross-section of the full model with the air box is shown in Figure 2-2.

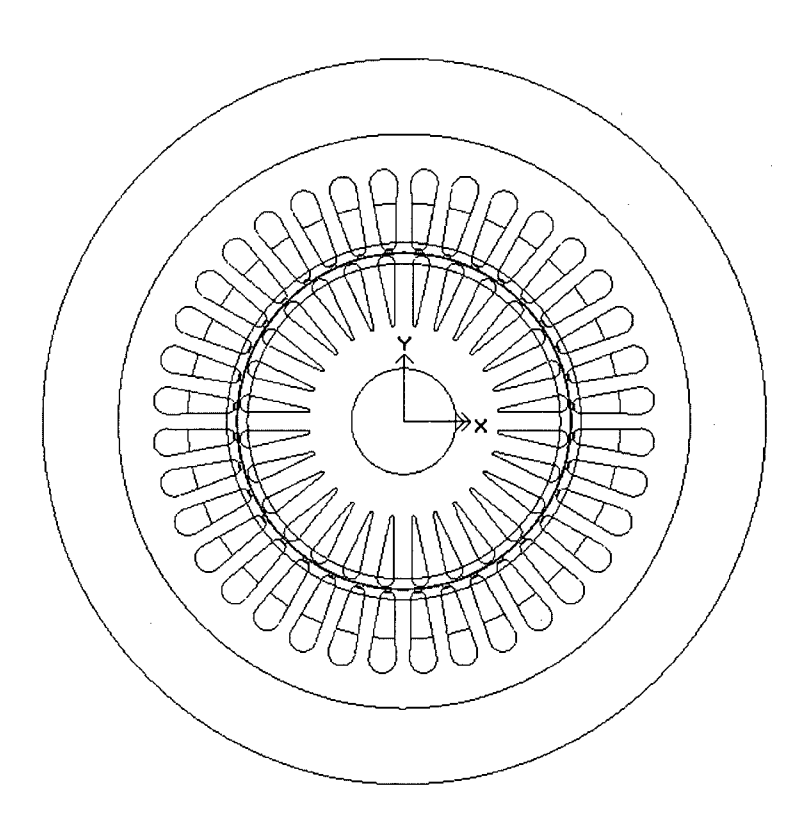


Figure 2-2 Cross-section of the induction motor

2.3.1.2 Air gap modeling

When using the transient with motion solver, a motion component needs to be created by grouping together the moving components (e.g. rotor, rotor bar, air gap). The motion source type for this component can be velocity driven, in which case movement is imposed by a user defined waveform of position or speed versus time; or it can be load driven, in which case the movement is obtained by solving the equations of motion. If the motion source is of the latter type, accurate magnetic force/torque calculation is critical in arriving at the right solution. For this reason, special attention is given to the modeling of the air region that surrounds the motion component.

As mentioned in Section 2.2.2.1, the force calculation method used by *MagNet* for electrical machines is based on the Maxell stress tensor method. Using this approach, the magnetic force in the induction motor is calculated by evaluating the field in the layer of *AIR* elements adjacent to the motion component. Since this field is in elements that are immediately adjacent to sharp corners of the stator and rotor teeth, high field errors are more likely to occur, leading to poorly accurate force or torque values. *MagNet* overcomes this problem by surrounding the body with a layer of *Virtual Air* material as shown Figure 2-3. This material has the same properties as air but is not used by *MagNet* as a separation region between bodies as the *AIR* material is. This *Virtual Air* shield allows the surface on which the force density is integrated to be pushed away from field singularities [37].

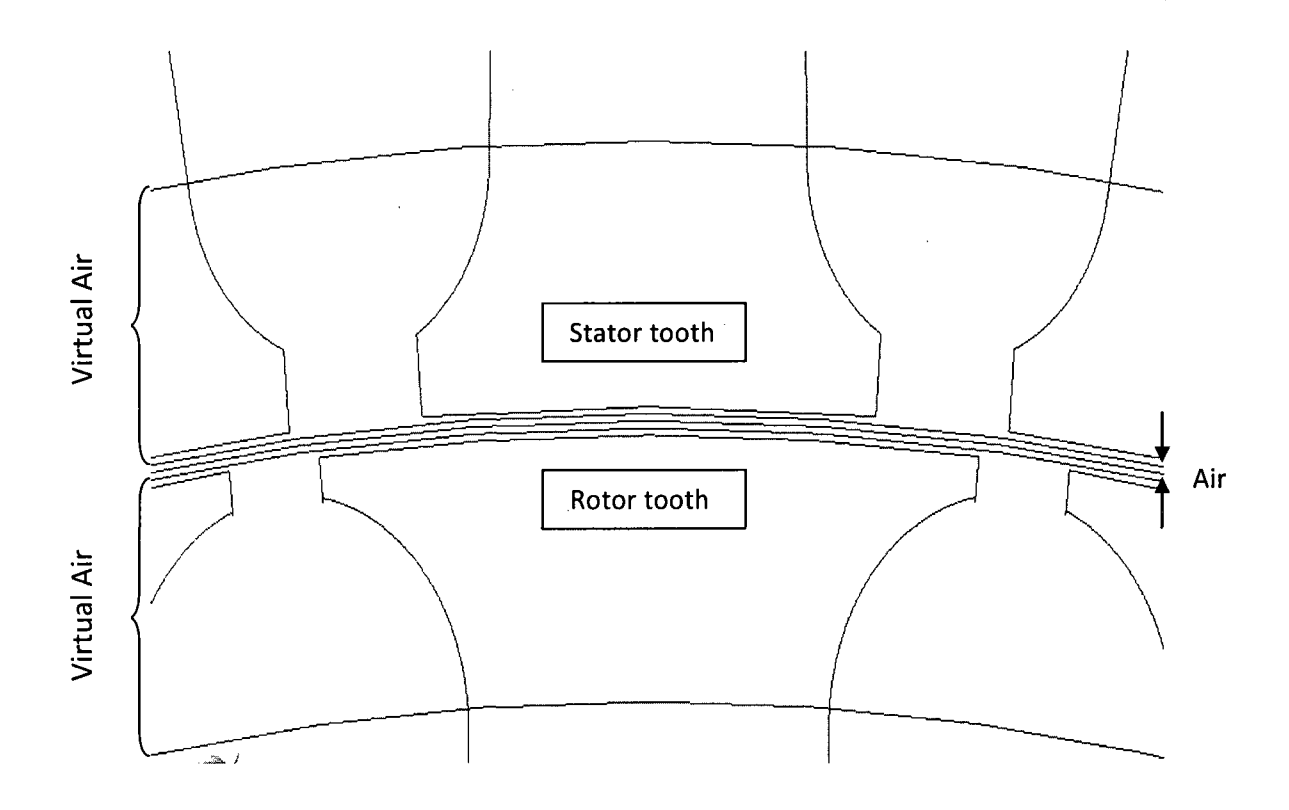


Figure 2-3 Virtual Air Shield Method

2.3.1.3 Periodicity

A model is periodic when its geometry, materials, and excitations repeat periodically. When such periodicity exists, the solution domain can be truncated in order to save on computer resources, by using periodicity constraints which effectively replace a contact with an unmodeled repeating part of the device. Periodicity can be of two types: *Even* or *Odd*. Even periodicity corresponds to the case where the polarities of the excitations are the *same* from one repeating section to the next. In this case, an even periodicity boundary condition can be used in order to keep only one repeating section in the model. On the other hand, odd

periodicity corresponds to the case where the polarities of the excitations alternate from one repeating section to the next. In this case, the model can be reduced by applying an odd periodicity boundary condition and keeping only the repeating section.

The induction motor that is modeled in this thesis exhibits odd periodicity with a periodicity angle of 90° because the geometry, materials, and excitations repeat every 90° and the polarities of the excitations alternate from one repeating section to the next. As a result, only the reduced portion of the model, shown in Figure 2-4, needs to be solved saving computing resources.

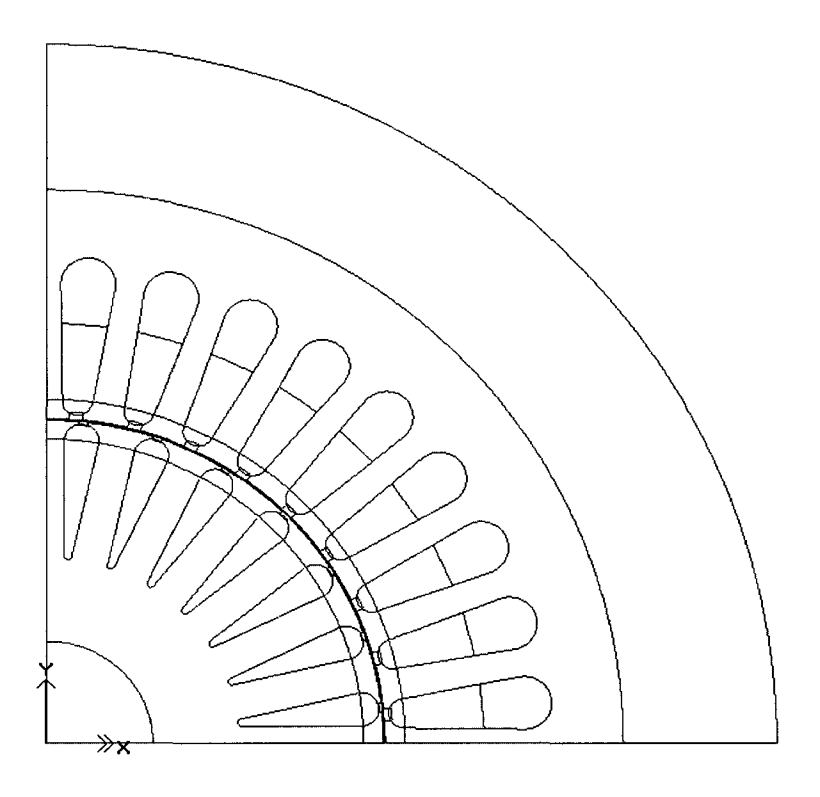


Figure 2-4 Quarter model of the induction motor

2.3.1.4 Boundary conditions

In the analysis of electromagnetic devices, boundary conditions are used to specify the behavior of the electromagnetic field on the outer surfaces of the device under study. The boundary conditions, together with the partial differential equations governing the phenomena of interest, form a well-posed boundary value problem for which a unique solution exists, and that can be solved using a numerical method such as the FEM.

Boundary conditions in *MagNet* can be classified as unary (Flux Normal, Flux Tangential, and Surface Impedance boundary conditions) and binary (Even and Odd Periodic boundary conditions). With the unary boundary conditions the field behavior is specified on a given surface/edge, whereas with the binary boundary conditions, a relationship between two surfaces/edges is specified.

In the case of the two-dimensional quarter induction motor modeled in this thesis, the Odd Periodic boundary condition is specified on the bottom outer edges of the stator and rotor air boxes that are shared with the unmodeled side of the motor. On all other outer edges of the stator and rotor air boxes, the Flux Tangential boundary condition is specified.

2.3.1.5 Coils and Circuits

The phase windings in the stator, and the rotor bars in the rotor cage of the induction motor are modeled as stranded and solid coils, respectively. In order to take into account the effects

of the end regions of the stator windings in the two-dimensional field analysis considered in this thesis, the stator end windings are modeled by means of external resistances whose values are calculated using empirical formulae. These resistors are then added to the electric circuit that is used to electrically connect the stator windings as shown in Figure 2-5.

When periodicity is invoked in order to solve a reduced portion of a model containing circuits, as is done in this thesis, the coils belonging to the un-modeled parts of the device must be removed from the circuits and connections added, so that the remaining coils and circuit components are subjected to the same current and voltage as in the complete, original circuits. If, for example, a voltage source is connected to series coils of which a certain number will be removed because they belong to an un-modeled part of the device, then the source voltage must be reduced in such a way that the remaining coils are subjected to the same voltage difference as they would be in the complete circuit. Similarly, broken series branches in the partial circuits are reconnected, using periodicity constraints, to allow for the same current to flow.

Consider, for example, the rotor bars of a rotary induction machine exhibiting even periodicity, and connected according to the standard squirrel-cage configuration. Since the current entering into each repeating group of coils is the same because of the even periodicity, the group of coils kept in the partial model should be connected together as they are in the complete model in order to allow that current to flow as it does in the complete model. If the periodicity is odd instead of even, any partly modeled two-dimensional conductor or circuit must be consistent

with the fact that the fields and signals should reverse when going from the modeled part of the device to one of its neighboring un-modeled parts.

As mentioned before, the squirrel-cage induction motor modeled in this thesis exhibits odd-periodicity with a periodicity angle of 90°. From the definition of odd periodicity, this implies that the voltage at a rotor bar's terminals is zero. Therefore, in order to properly express the squirrel cage configuration when modeling only one of the repeating sections of the odd-periodic motor, the rotor bars should be explicitly short-circuited.

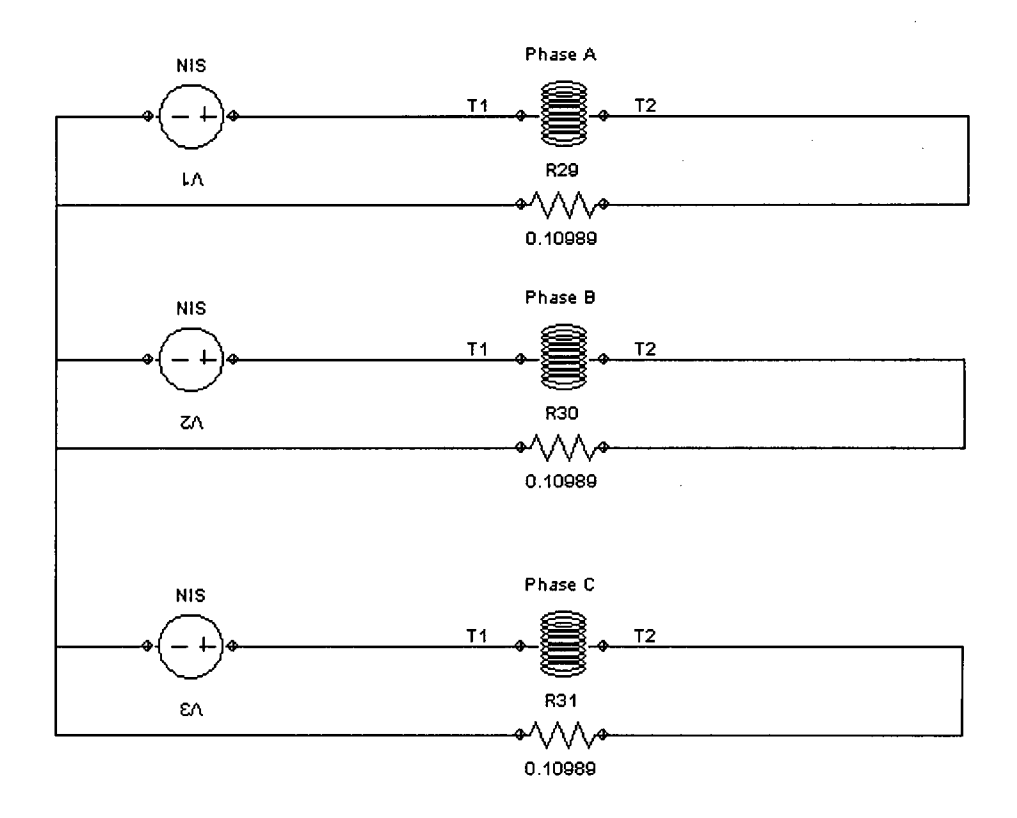


Figure 2-5 Stator winding circuit

2.3.1.6 Meshing

In the two-dimensional finite element analysis, the computational domain is divided into a mesh of triangular-shaped elements. The field inside each of these elements is represented by a polynomial function with unknown coefficients. The accuracy of the solution depends upon the nature of the field and the size of the mesh elements. In regions where the direction or magnitude of the field changes rapidly, small elements are required for high accuracy.

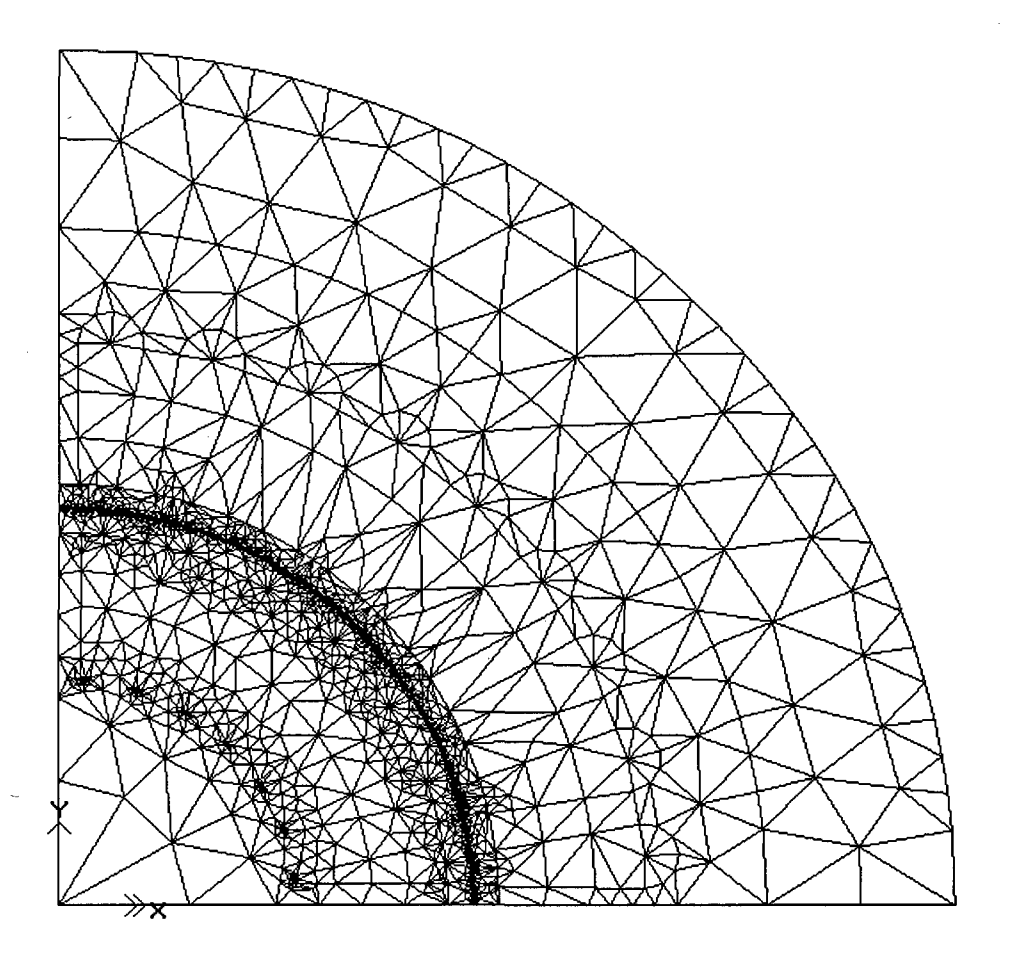


Figure 2-6 Meshed model of the induction motor

2.3.2 Simulation of the no-load test

In this test, stator currents are imposed on the stator windings and the non-linear behavior of the magnetizing inductance is computed. A series of simulations are carried out parameterizing the stator current. The non linear characteristic of the iron is used in the simulation. Figure 2-7 shows the flux plot during the no-load test.

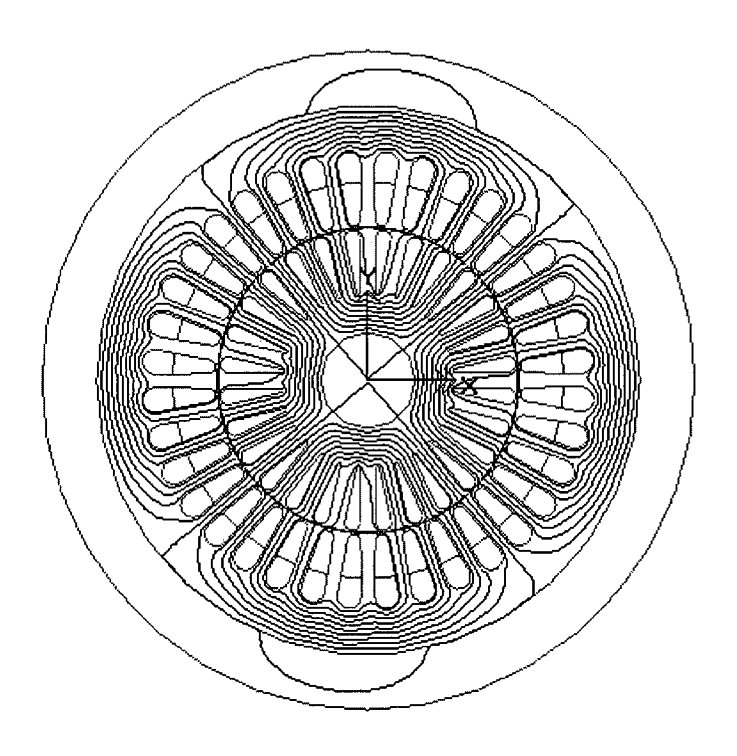


Figure 2-7 Flux plot under no-load condition

The magnetizing inductance of the induction motor is computed as,

$$L_m = \frac{\lambda_s}{i_s} \tag{2.16}$$

where λ_s is the stator flux linkage vector and i_s is the stator current vector.

The phase flux linkage and the magnetizing inductance as a function of the parameterized stator current are shown in Figure 2-8 and Figure 2-9, respectively.

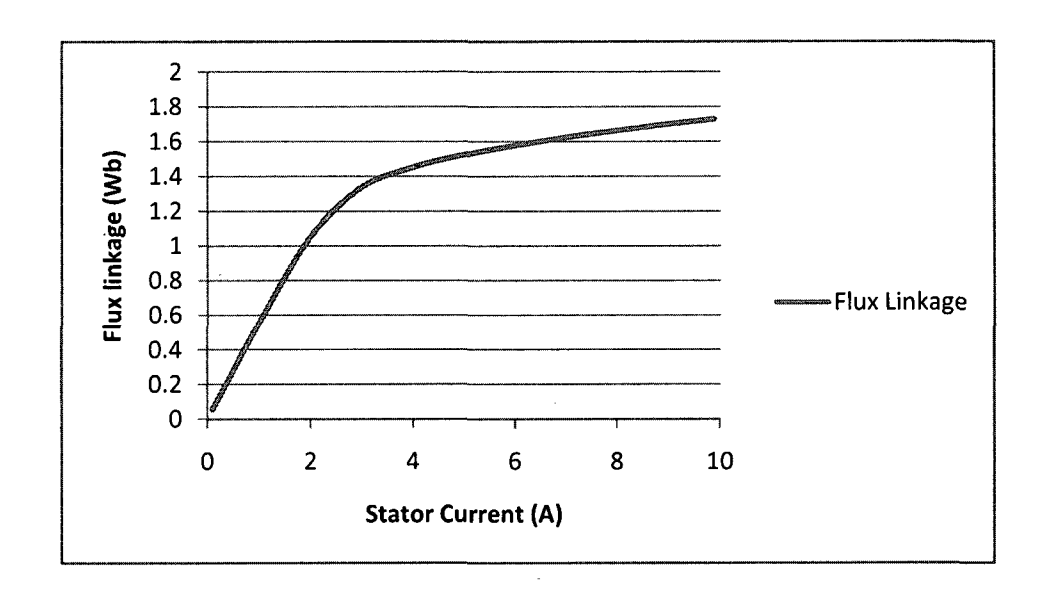


Figure 2-8 Flux-linkage versus stator current

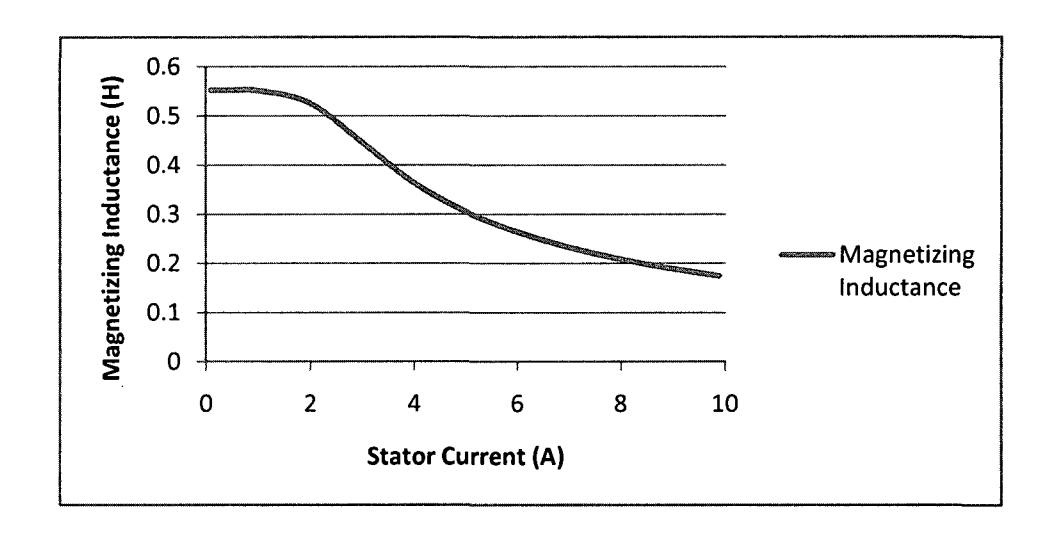


Figure 2-9 Magnetizing inductance vs. current

Another way to calculate the magnetizing inductance uses the total stored magnetic energy, W_{tm} . This energy can be obtained from the non-linear field solution using the energy density, w,

$$w = \int_0^B H \cdot dB \tag{2.17}$$

The total stored energy then becomes

$$W_{tm} = \iiint_{vol} w dvol \tag{2.18}$$

The magnetizing inductance is given by [38],

$$L_m = \frac{2}{3} \frac{W_{tm}}{i_s^2} \tag{2.19}$$

In this thesis, the above method (i.e. Equation (2.19)) of calculating the magnetizing inductance is used.

The results of the no-load simulation are summarized in Appendix A.

2.3.3 Simulation of the locked-rotor test

The simulation of this test is carried out using *MagNet's* time-harmonic solver imposing a fixed current on the stator windings. A series of simulations is carried out at various frequencies so as to determine the dependence of the rotor parameters on the operating frequency.

In these simulations the iron core is assumed to be linear, since the field quantities need to vary sinusoidally in order to be able to use phasor quantities. The corresponding magnetizing inductance of the equivalent circuit of Figure 2-1 is fixed to its linear value. This assumption does not affect the computation since the main purpose of this test is to compute the rotor parameters.

Figure 2-10 and Figure 2-11 show the flux plots during the locked rotor test at two different slip frequencies: at 50 Hz and at 10 Hz, respectively.

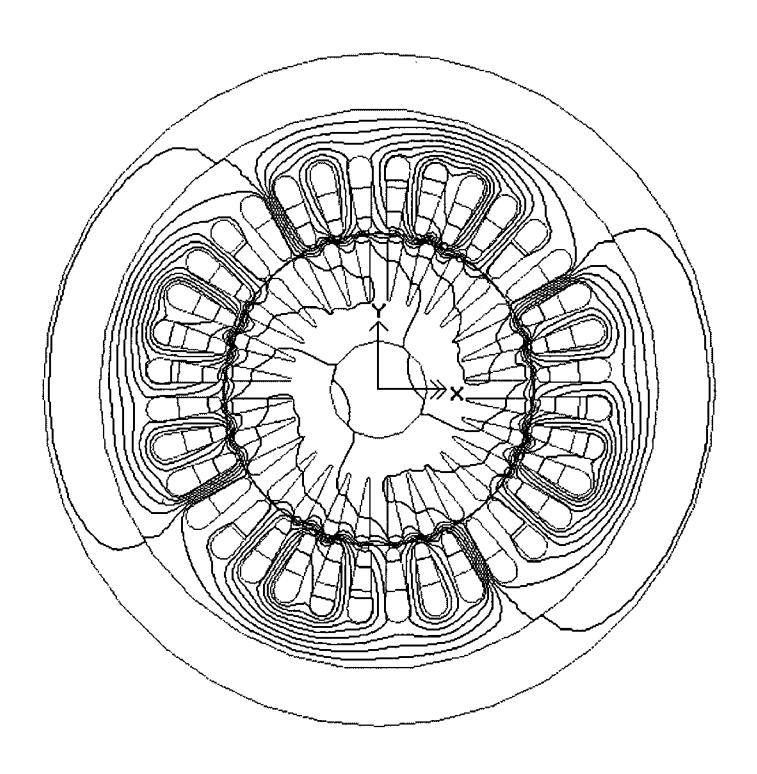


Figure 2-10 Locked-rotor flux-plot for 50 Hz

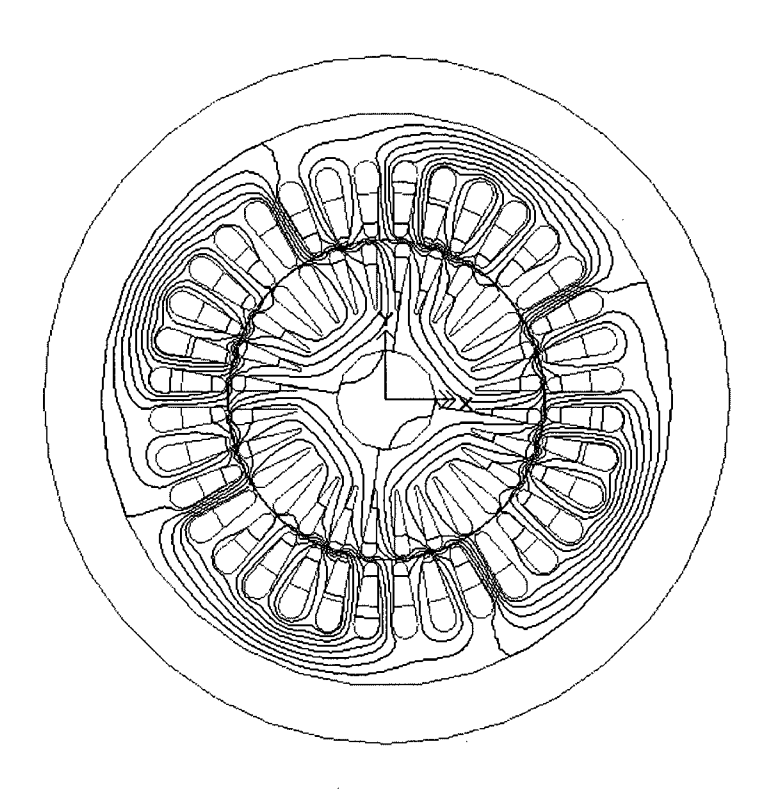


Figure 2-11 Locked-rotor flux-plot for 10 Hz

Figure 2-12 shows the computed torque as a function of the rotor frequency. It should be noted here that this torque is obtained using a constant current source, fixed in all simulations. It is different from the torque obtained at fixed voltage to plot the mechanical characteristic of the machine.

The torque can be found in two ways; the first requires the computation of the Maxwell stress tensor along a line within the air gap of the motor. The second is derived from the fact that the torque is proportional to the power transferred from the stator to rotor. The torque, then, can be determined from the ratio of the rotor power losses, P_r , and the synchronous speed, ω_e , as shown below

$$T_e = \frac{P_r}{\omega_e} \tag{2.20}$$

where

$$\omega_e = 2\pi\,f/P$$

f is the frequency adopted in the simulation, and

P is the number of pole pairs.

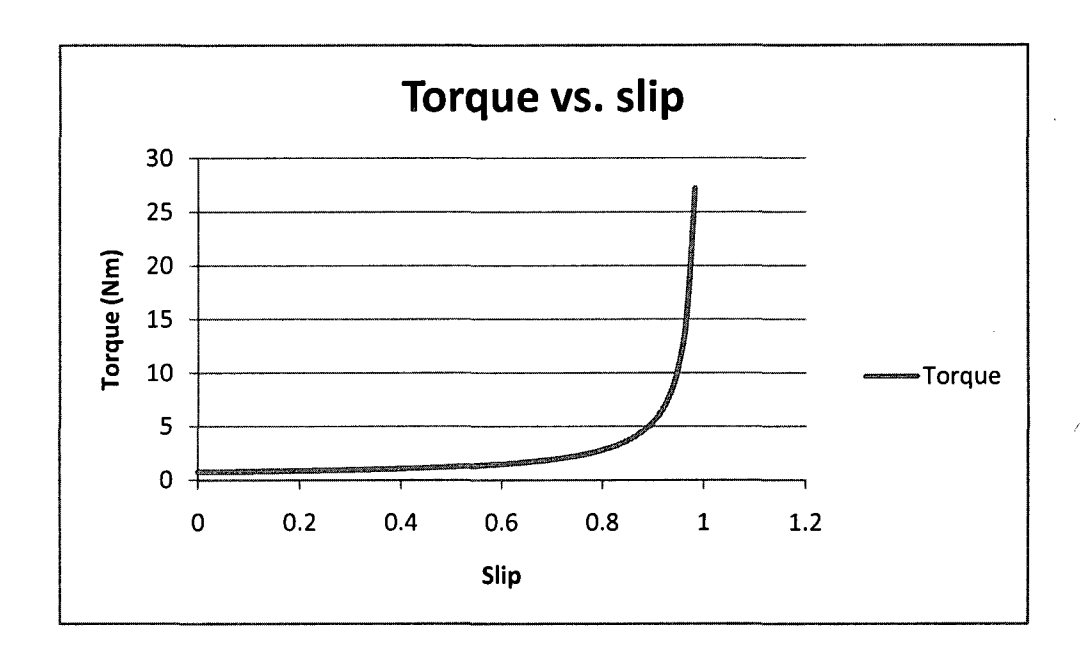


Figure 2-12 Torque vs. slip

The rotor parameters are computed as follows:

$$R_{eq} = \frac{P_r}{3I_{srms}^2} \tag{2.21}$$

$$L_{eq} = \frac{2}{3} \frac{W_m}{I_{srms}^2}$$
 (2.22)

where I_{srms} is the RMS stator current used in the simulation.

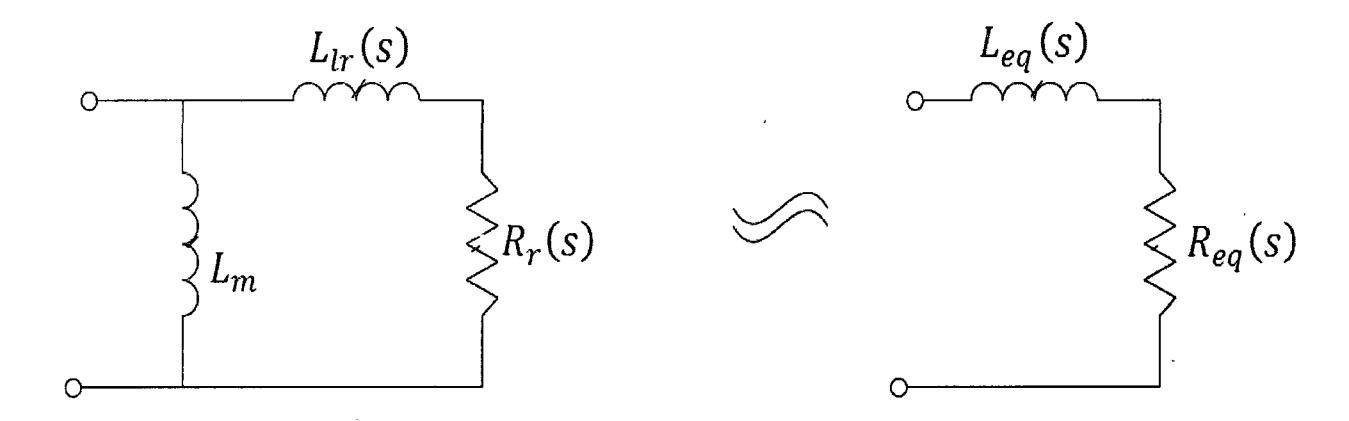


Figure 2-13 Equivalent circuits corresponding to the locked-rotor simulation

Considering the approximation shown in Figure 2-13

$$L_{l} = L_{m} \frac{L_{eq} (L_{m} - L_{eq}) - (R_{eq}/\omega)^{2}}{(L_{m} - L_{eq})^{2} + (R_{eq}/\omega)^{2}}$$
(2.23)

$$R_r = L_m \frac{(L_m + L_l)}{(L_m - L_{eq})} \tag{2.24}$$

where L_l is the total leakage inductance ($L_l = L_{ls} + L_{lr}$)

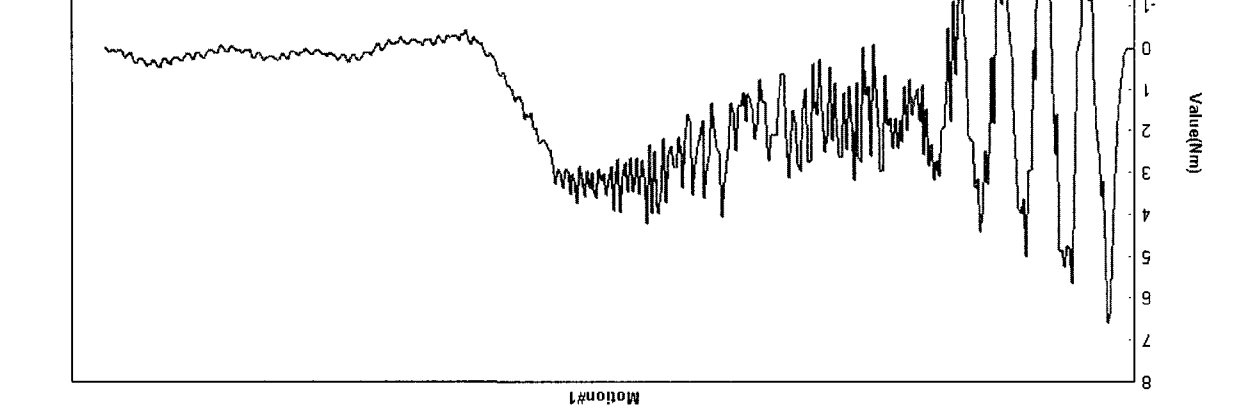
The results of the locked-rotor simulations are summarized in Appendix A.

2.3.4 Transient field analysis

While most of the analyses of the induction machine can be carried out using the static and time-harmonic solvers, there are some conditions that require the use of the transient with motion solver. These conditions occur when

- it is necessary to model the induced currents due to motional effects,
- the power supply to the machine is not sinusoidal.
- it is necessary to couple the induction machine with other mechanical components, and
- it is preferable to solve a parameterized sequence of static problems using the transient with motion solver (the parameterized quantity must be shift or rotation)

In this thesis the start-up condition of the induction motor is analyzed. Since it is necessary to model the effects of motion in order to carry out this analysis, *MagNet's* transient with motion solver is used. The motion component is set to be load driven because the velocity is not known and it varies with time as a result of the generated electromagnetic field. Figure 2-14 and Figure 2-15 shows the rotor speed and the electromagnetic torque, respectively, as a function of time for a voltage driven model.



Magnetic Torque

Figure 2-14 Electromagnetic torque vs. time

(sm) əmiT



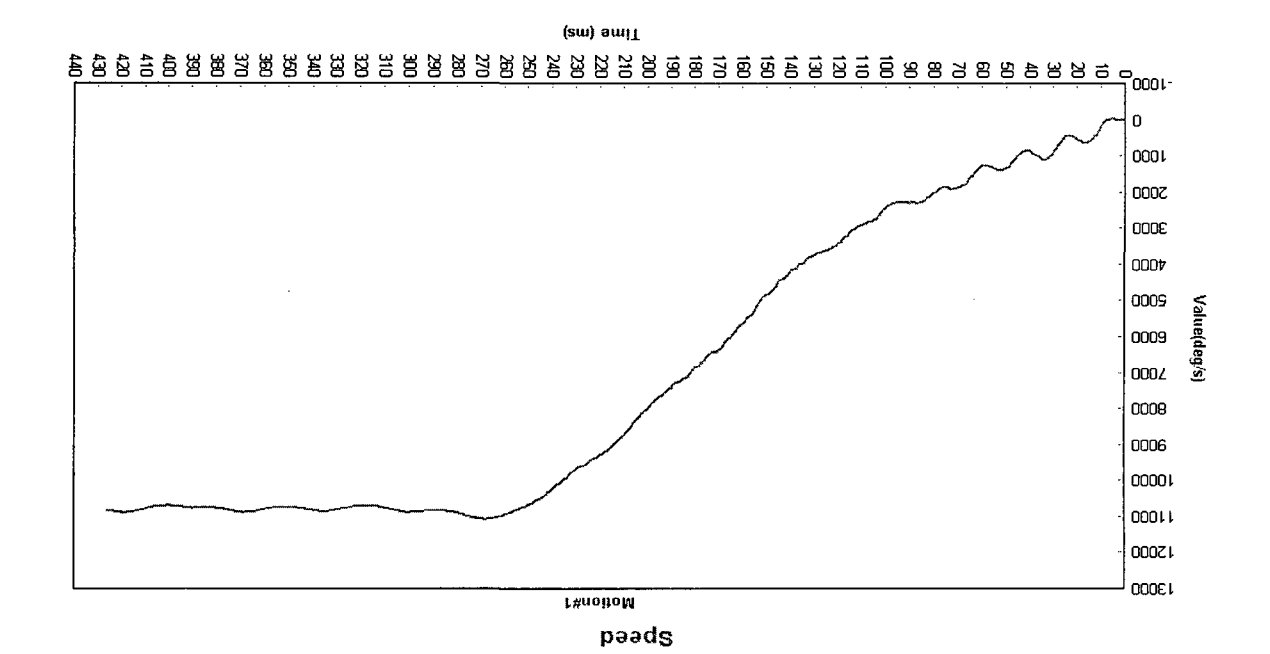


Figure 2-15 Mechanical speed vs. time

3 Field Oriented Control of Induction Motors

The purpose of this chapter is to discuss the theoretical background and Simulink implementation of the field oriented controlled induction motor drive. It begins with a presentation of a dynamic model of the induction motor that is based on the *dq-axes* theory. Then a brief review of the field orientation principle is given. This is followed by an overview of the FOC drive system and an illustration of its Simulink implementation. Finally, the *dq-axes* model of the induction motor modeled in Section 2.3 is used in a Simulink simulation of an indirect FOC drive system and the results are presented.

3.1 Two-axes representation of the induction motor

The two axes (dq) circuit model of the induction motor is one of the commonly used dynamic models in control synthesis. The main advantage of using this model is the controlled quantities such as voltages and currents become dc values. This simplifies the expressions for control purposes and simple linear controller can be used. One way of deriving this model is to start from the space vector model of the induction motor [39]. This is composed of three equations — These are the voltage equations, the flux equations, and the motion equation. The voltage equations are given by,

$$v_s = R_s i_s + p \lambda_s + j \omega \lambda_s$$

$$v_r = R_r i_r + p \lambda_r + j (\omega - \omega_r) \lambda_r$$
(3.1)

where

 v_{s} and v_{r} are the stator and rotor voltage vectors, respectively,

 $oldsymbol{i_s}$ and $oldsymbol{i_r}$ are the stator and rotor current vectors, respectively

 λ_s and λ_r are the stator and rotor flux linkage vectors, respectively, and

p is d/dt

The flux linkage equations are,

$$\lambda_s = L_s i_s + L_m i_r$$
$$\lambda_r = L_r i_r + L_m i_s$$

where (3.2)

 $L_s = L_{ls} + L_m$ is the stator self inductance, and

 $L_r = L_{lr} + L_m$ is the rotor self inductance

And, the motion equation is given by

$$\frac{J}{P}p\omega_r = T_e - T_L$$

$$T_e = \frac{3P}{2}\operatorname{Re}(j\lambda_s i_s^*) = -\frac{3P}{2}\operatorname{Re}(j\lambda_r i_r^*)$$
(3.3)

where

J, is the moment of inertia of the rotor,

P, is the number of pole pairs.

 ω_r , is the angular velocity/mechanical speed of the rotor,

 T_e , is the electromagnetic torque, and

 T_L , is the external torque.

Now, if the space vectors in equations (3.1), (3.2), and (3.3) are decomposed into the dq-axes components as shown in equation (3.4),

$$v_s = v_{ds} + jv_{qs};$$
 $i_s = i_{ds} + ji_{qs};$ $\lambda_s = \lambda_{ds} + j\lambda_{qs}$
 $v_r = v_{dr} + jv_{qr};$ $i_r = i_{dr} + ji_{qr};$ $\lambda_r = \lambda_{dr} + j\lambda_{qr}$ (3.4)

and, substituted back into equations (3.1) and (3.2), the dq-axes voltages will be,

$$\nu_{ds} = R_s i_{ds} + p \lambda_{ds} - \omega \lambda_{ds}
\nu_{qs} = R_s i_{qs} + p \lambda_{qs} + \omega \lambda_{ds}
\nu_{dr} = R_r i_{dr} + p \lambda_{dr} - (\omega - \omega_r) \lambda_{dr}
\nu_{qr} = R_r i_{qr} + p \lambda_{qr} + (\omega - \omega_r) \lambda_{dr}$$
(3.5)

and, the dq-axes flux linkages,

$$\lambda_{ds} = L_{ls}i_{ds} + L_{m}(i_{ds} + i_{dr})
\lambda_{qs} = L_{ls}i_{qs} + L_{m}(i_{qs} + i_{qr})
\lambda_{dr} = L_{lr}i_{dr} + L_{m}(i_{ds} + i_{dr})
\lambda_{qr} = L_{lr}i_{qr} + L_{m}(i_{qs} + i_{qr})$$
(3.6)

Replacing the space vectors in the electromagnetic torque equation (3.3) with the *dq-axes* components of equations (3.4) and (3.6) results in one of the following equations,

$$T_{e} = \begin{cases} \frac{3P}{2} (i_{qs}\lambda_{ds} - i_{ds}\lambda_{qs}) \\ \frac{3PL_{m}}{2} (i_{qs}i_{dr} - i_{ds}i_{qr}) \\ \frac{3PL_{m}}{2L_{r}} (i_{qs}\lambda_{dr} - i_{ds}\lambda_{qr}) \end{cases}$$
(3.7)

The equivalent circuit of the dq-axes model of the induction motor is shown in Figure 3-1

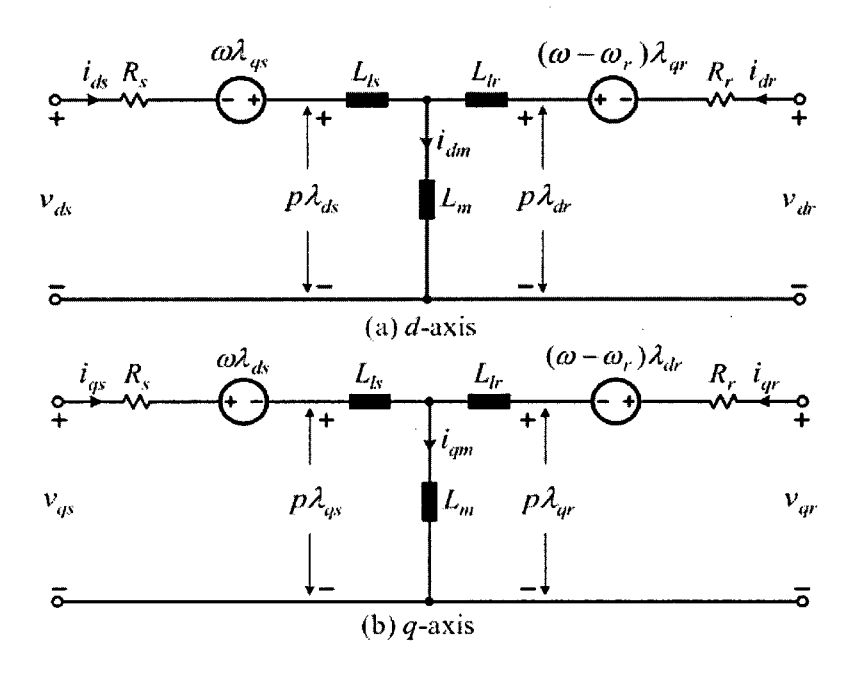


Figure 3-1 Equivalent circuit of the dq-axes model of the induction motor

3.2 Principle of field orientation

The reason that the dc motor drive has excellent dynamic performance is the stator magnetic field and electromagnetic torque of the motor can be controlled separately. This is because the torque in dc motors is developed by the interaction of two perpendicular magnetic fields. One of these fields is generated by the field current i_f in the stator winding, and the other is produced by the armature current i_a . The developed torque can be expressed as

$$T_e = K_a \lambda_f i_a \tag{3.8}$$

where K_a is an armature constant and λ_f is the flux produced by i_f . From this equation it is obvious that if λ_f is kept constant by keeping i_f constant, the torque, T_e , can be directly controlled by i_a .

The objective of field orientation in induction motor drives is to emulate this dc drives feature.

Using a proper field orientation the stator current is decomposed into a flux producing component and a torque producing component. These two components are then controlled separately as is the case in dc drives.

Depending on the flux vector used to align with the synchronous reference frame, the field orientation can be classified into rotor flux, stator flux, and air gap flux orientations [40]. Since the rotor flux orientation is extensively used in induction motor drives, the discussion henceforth is restricted to this scheme only. The rotor flux orientation is achieved by aligning

the *d-axis* of the synchronous reference frame with the rotor flux vector as shown in Figure 3-2.

The resultant d and q axes rotor flux components are

$$\lambda_{ar} = 0 \text{ and } \lambda_{dr} = \lambda_r \tag{3.9}$$

where λ_r is the magnitude of λ_r

Substituting equation (3.9) into the last equation of (3.7) gives

$$T_e = \frac{3PL_m}{2L_r} \lambda_{dr} i_{qs} = \frac{3PL_m}{2L_r} \lambda_r i_{qs}$$
 (3.10)

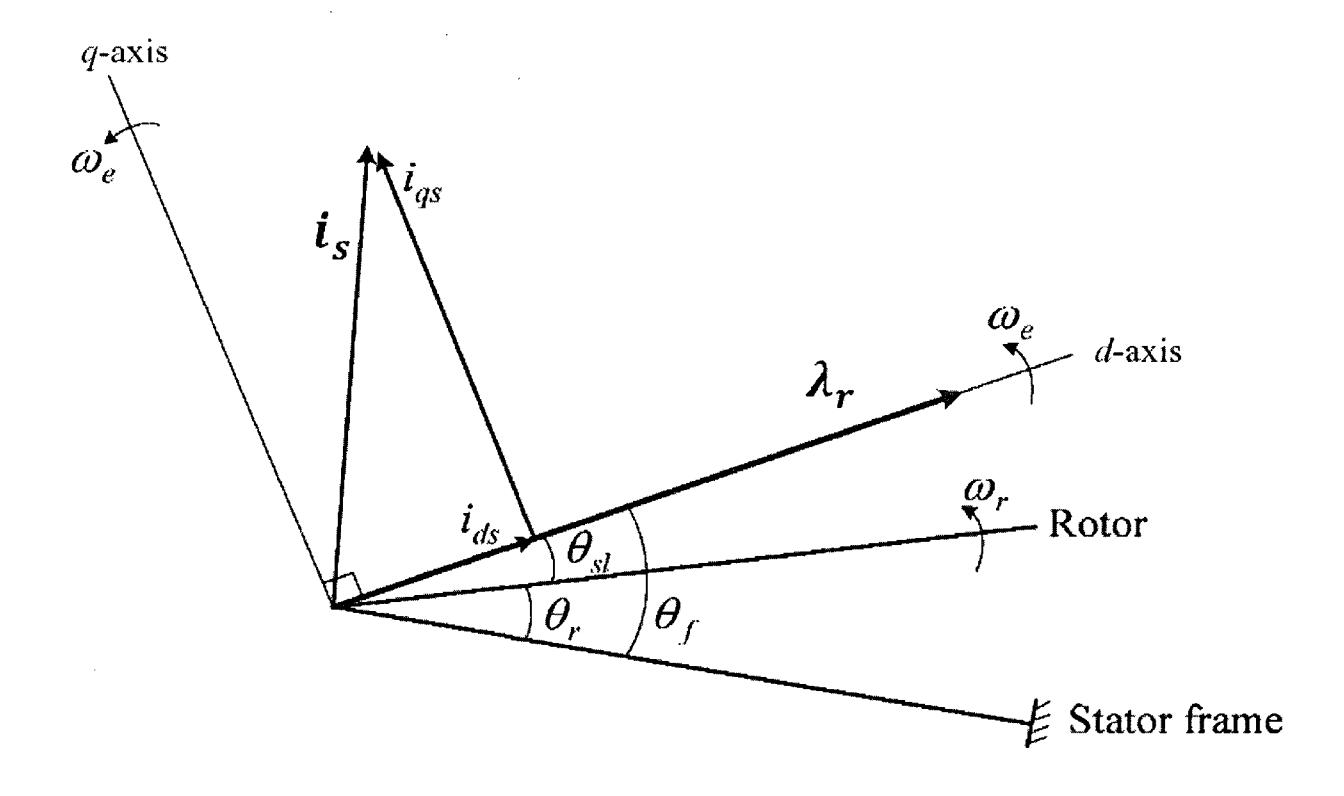


Figure 3-2 Rotor flux field orientation

Equation (3.10) shows that with the rotor field orientation, the torque expression for the induction motor is similar to that of a dc motor. If λ_r can be kept constant during the motor operation, the developed torque can be directly controlled by the q-axis stator current i_{qs} .

The stator current vector, i_s , in Figure 3-2 can be resolved into two components along the dq-axes. The d-axis current i_{ds} is referred to as the flux producing current while the q-axis current i_{qs} , which is perpendicular to i_{ds} , is the torque producing current. In the field-oriented control, i_{ds} is normally kept at its rated value while i_{qs} is controlled independently. With the decoupled control for i_{ds} and i_{qs} , a high-performance drive can be realized.

One of the key issues associated with the rotor flux-oriented control is to accurately determine the rotor flux angle, θ_f , for field orientation. Various schemes can be used to find θ_f . For instance, it can be calculated from measured stator voltages and currents, or it can be found from

$$\theta_f = \theta_r + \theta_{sl} \tag{3.11}$$

where θ_r and θ_{sl} are the measured rotor position and calculated slip angle, respectively.

3.3 Description of the FOC drive system

Depending on how the rotor flux angle, θ_f , is obtained, the field oriented control can be classified as direct or indirect field-oriented control. If θ_f is obtained by using flux-sensing

devices embedded inside the motor or using measured motor terminal voltages and currents, the method is referred to as direct field-oriented control (DFOC) [14]. On the other hand, if θ_f is acquired from the measured rotor position angle, θ_r , and calculated slip angle, θ_{sl} , as shown in equation (3.5), this scheme is known as indirect field oriented control (IFOC) [15].

In this thesis, the indirect field oriented scheme is considered and the discussion hereafter focuses on this FOC type only. The power electronic converter used is a current controlled voltage source inverter. A general block diagram of an induction motor drive with rotor flux oriented control is shown in Figure 3-3 and the Simulink implementation of its main parts is illustrated in subsequent sections.

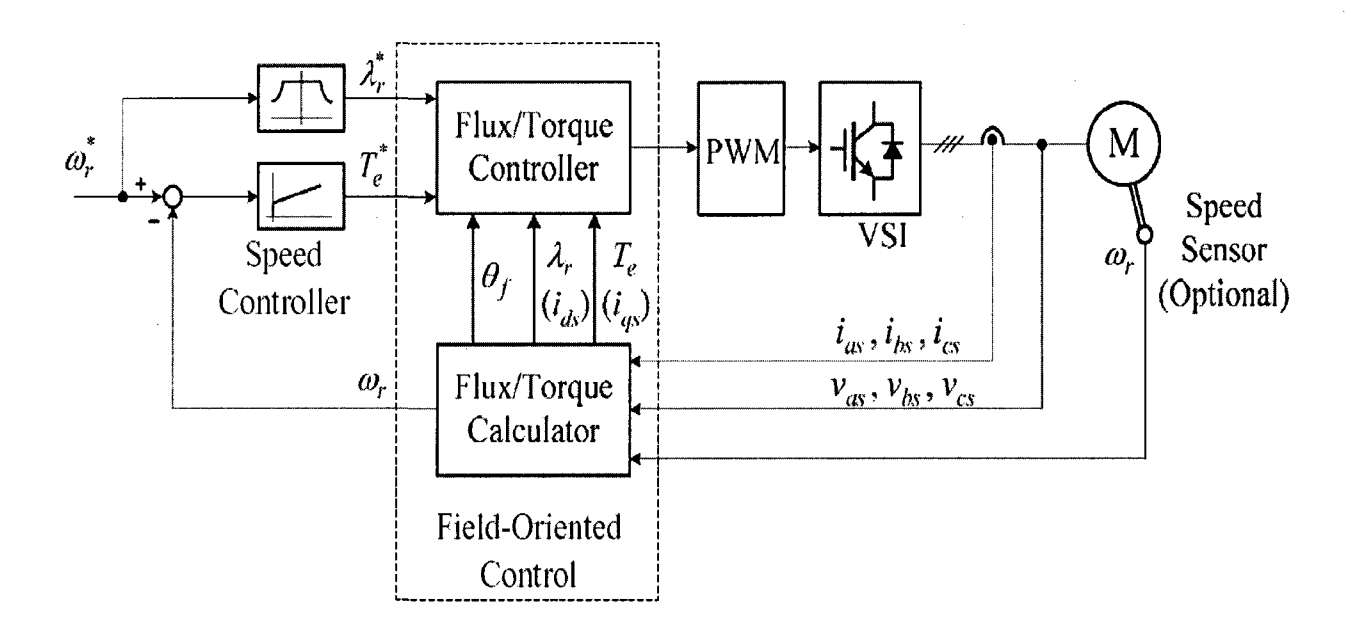


Figure 3-3 Overview of FOC drive system [39]

3.3.1 Speed controller

The speed controller used is a proportional integral (PI) controller and is implemented in Simulink as shown in Figure 3-4. Its purpose is to generate the torque reference T_e^* based on the reference speed ω_r^* and the measured or estimated rotor speed ω_r .

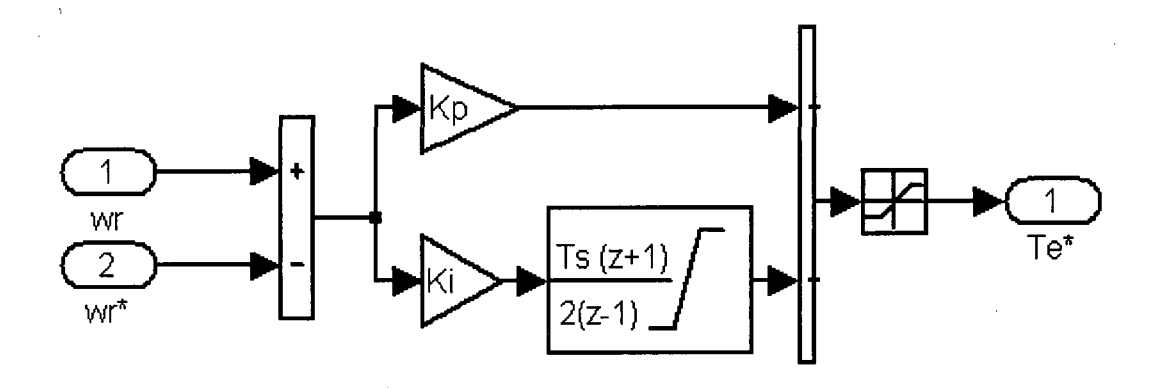


Figure 3-4 Speed - PI controller

3.3.2 Flux/Torque calculator

Based on the measured stator voltages and currents and the motor model, the flux/torque calculator of the drive system computes —

- 1) The rotor flux angle $\,\theta_f$ for field orientation,
- 2) The rotor flux magnitude λ_r or the flux producing current i_{ds} ,
- 3) The electromagnetic torque T_e or the torque producing current i_{qs} , and
- 4) The rotor speed ω_r (if the drive is sensorless)

3.3.2.1 Rotor flux angle

The rotor flux angle θ_f is found by integrating the sum of the rotor speed, ω_r , and the angular slip frequency, ω_{sl} , as shown below

$$\theta_f = \int_{t_1}^{t_2} (\omega_r + \omega_{sl}) dt \tag{3.12}$$

The angular slip frequency is derived using the following equation [39]

$$\omega_{sl} = \frac{L_m}{\tau_r \lambda_r} i_{qs} \tag{3.13}$$

where au_r is the rotor time constant, defined by

$$\tau_r = \frac{L_r}{R_r} \tag{3.14}$$

The Simulink block that performs the above calculations is shown in Figure 3-5.

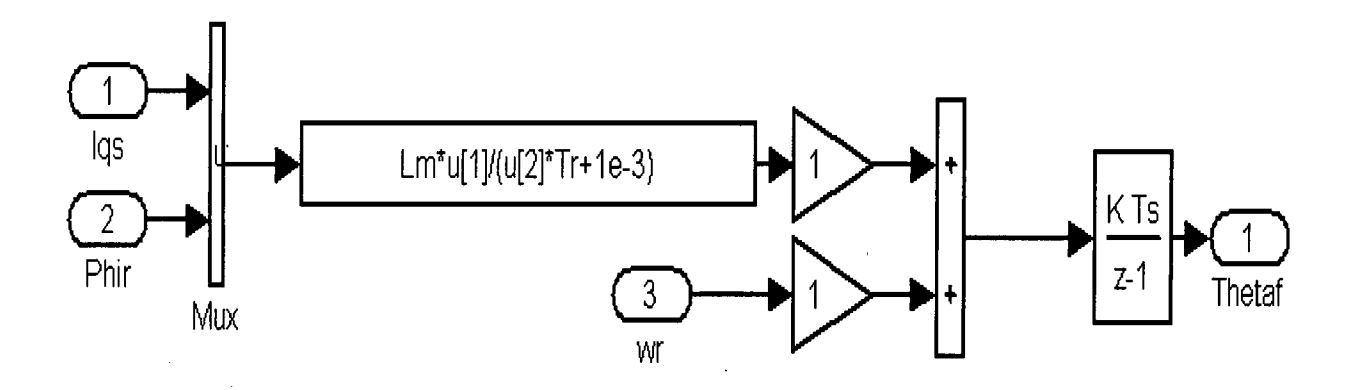


Figure 3-5 Rotor flux angle calculation block

3.3.2.2 Stator d-axis and q-axis currents

The stator *d-axis* and *q-axis* currents, which are the torque and flux producing currents respectively, are calculated by transforming the measured stator phase currents into the *dq-axes*. The matrix that performs this transformation is,

$$\begin{bmatrix}
i_a \\
i_b \\
i_c
\end{bmatrix} = \begin{bmatrix}
\cos \theta & -\sin \theta \\
\cos(\theta - 2\pi/3) & -\sin(\theta - 2\pi/3) \\
\cos(\theta - 4\pi/3) & -\sin(\theta - 4\pi/3)
\end{bmatrix} \cdot \begin{bmatrix} i_d \\ i_q \end{bmatrix}$$
(3.15)

The Simulink implementation of this operation is shown in Figure 3-6.

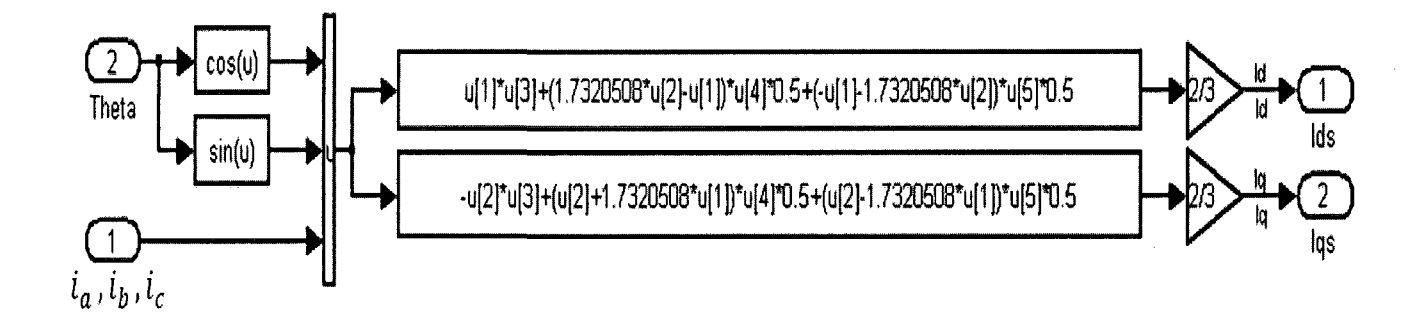


Figure 3-6 ABC - dq axes transformation

3.3.3 Flux/Torque controller

This section of the drive system calculates the stator reference currents using the rotor flux reference, λ_r^* , which is normally kept constant to its nominal value up to the rated speed of the

motor, and the torque reference, T_e^* , obtained from the speed controller. The calculated reference currents, along with the measured stator currents, are then sent to the Pulse Width Modulation (PWM) block to determine the gate signals for the inverter to adjust its output voltage and frequency. This particular PWM technique is called Hysteresis-band PMW and its method of operation is shown in Figure 3-7. Other common PWM techniques that are available depending on the type of inverter and control scheme employed include, Carrier-Based Sinusoidal PWM, Space Vector PWM, and Selected Harmonic Elimination PWM [41].

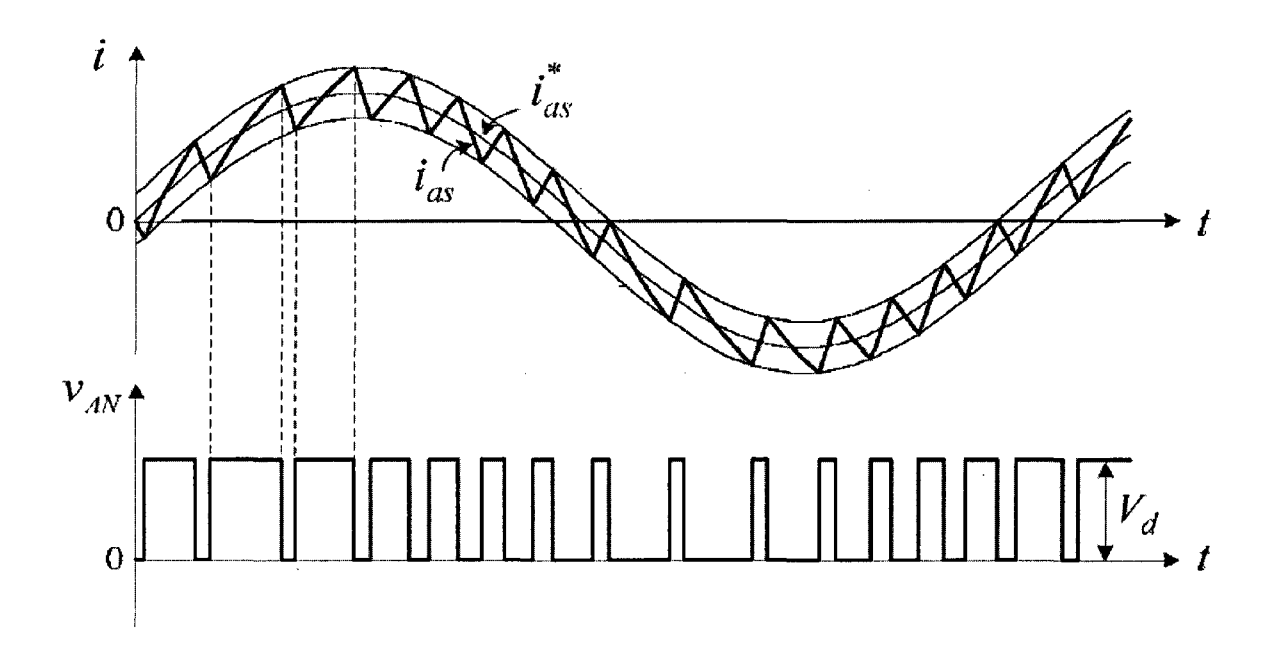


Figure 3-7 Hysteresis-band PWM

The Simulink implementation of the Hysteresis-band PWM consists of three hysteresis controllers and is shown in Figure 3-8.

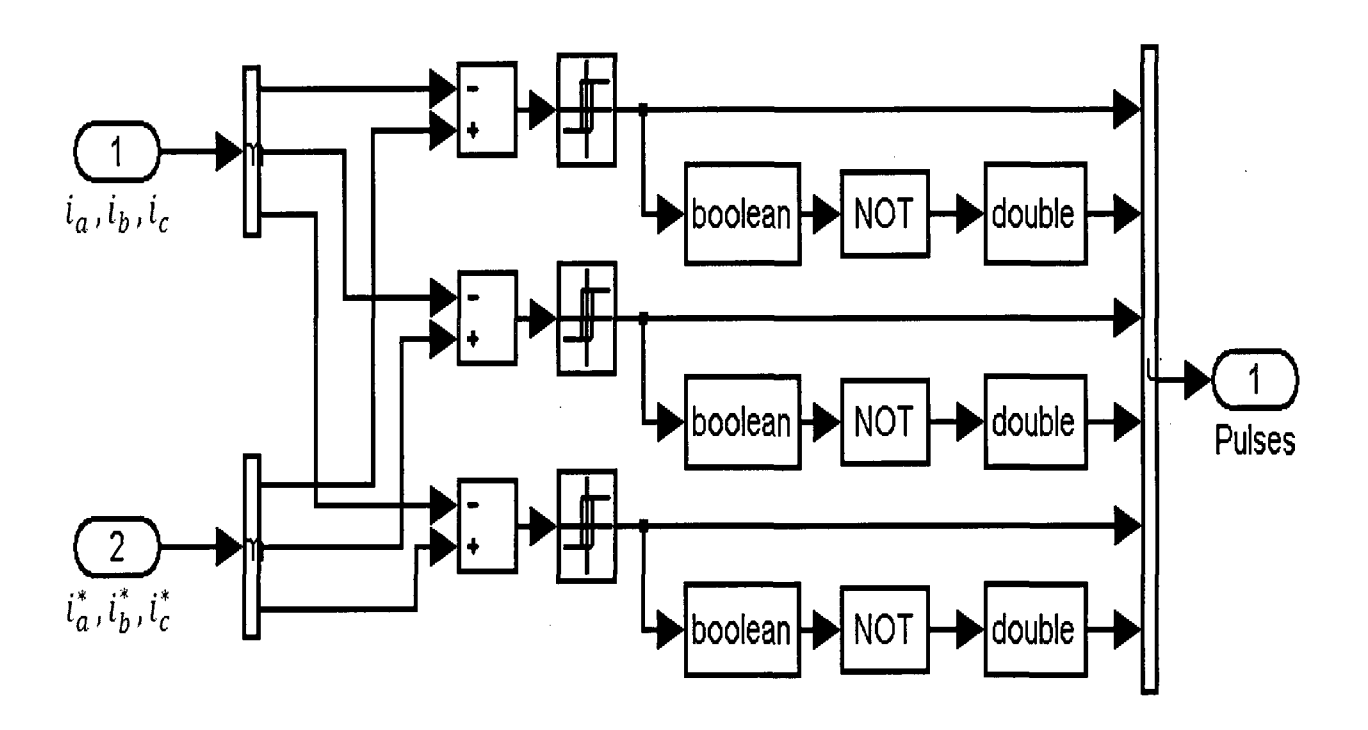


Figure 3-8 Simulink implementation of the Current regulator

3.4 Simulation results

In this section, an indirect field oriented controlled induction motor drive system is simulated in Simulink. The induction motor used in this drive is the same motor that was modeled in section 2.3, but here the *dq-axes* model, which is constructed using the lumped parameters (Table 3.1) of the motor, is used. The dynamic performance of the drive, i.e. speed regulation performance

versus reference and load torque changes, is studied by applying two changing operating conditions to the drive: a step change in speed reference and a step change in load torque.

Values
1.5894 Ω
1.419e-2 H
0.80755 Ω
1.419e-2 H
0.1611 H

Table 3.1 Lumped parameters of the induction motor

In the first simulation, the motor is started with a speed reference of $120 \, rad/s$ and with no load. The motor speed, electromechanical torque, and stator currents observed during the starting of the induction motor drive (the start up) are shown in Figure 3-9.

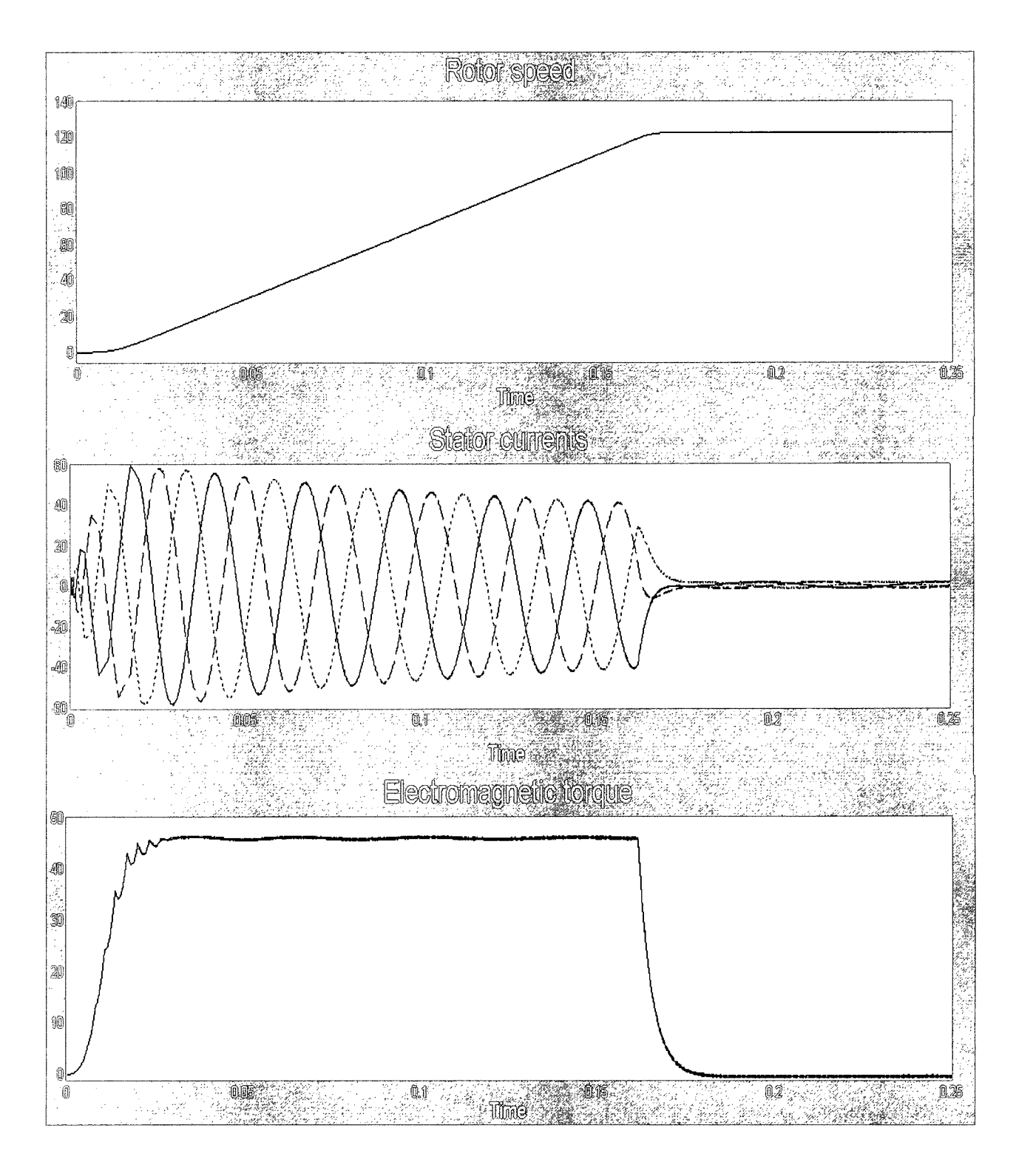


Figure 3-9 Waveforms of speed, current, and torque at start-up

In the second simulation, a load is applied to the motor while it is in steady state running at a speed of $120 \ rad/s$. The response of the induction motor drive to this load change is shown in Figure 3-10.

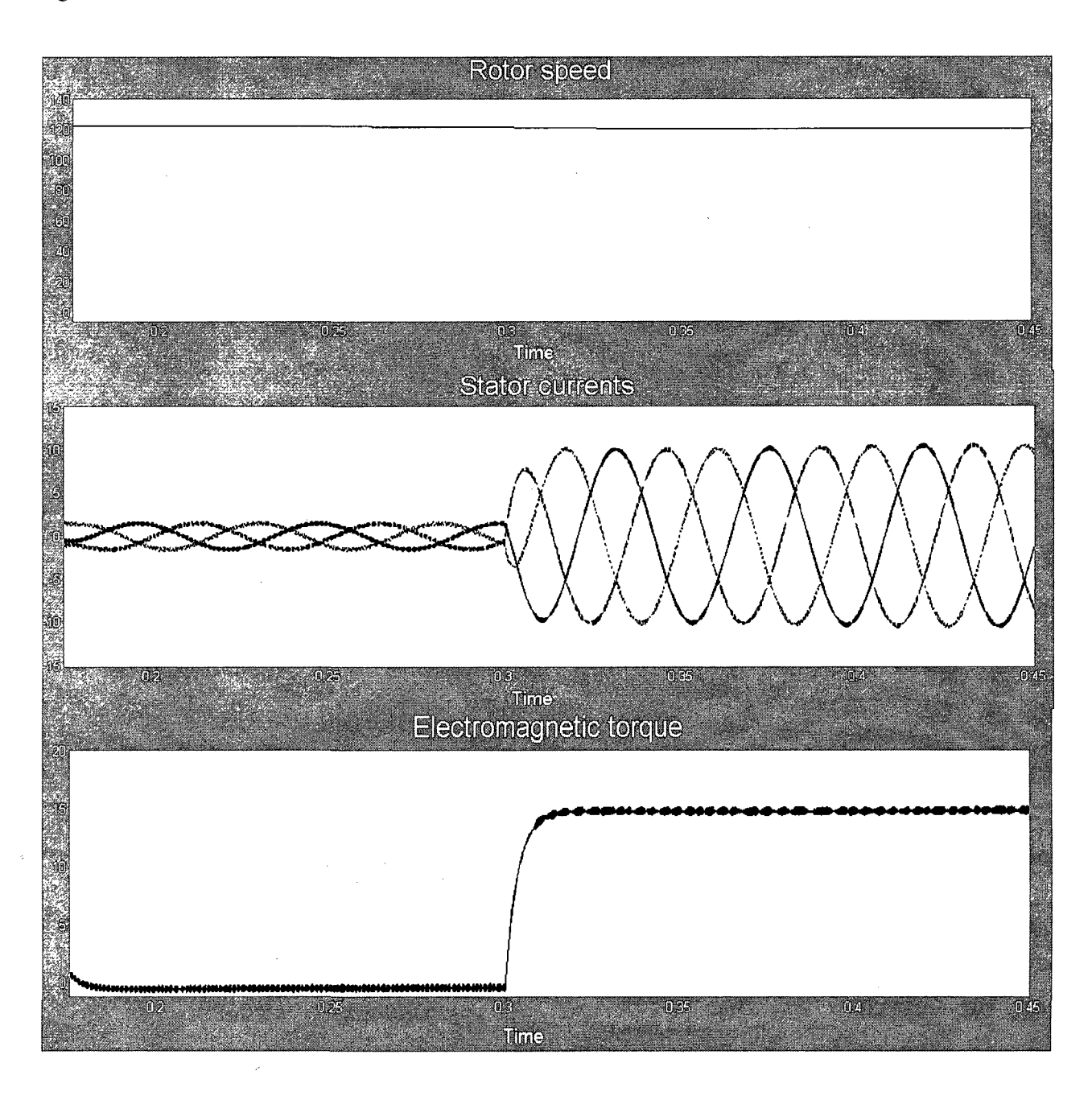


Figure 3-10 Waveforms of speed, current, and torque during load change

From the simulation results presented above, it can be observed that the field oriented scheme gives the induction motor drive superior dynamic performance compared to a scalar control scheme. As seen in Figure 3-9 and Figure 3-10, the drive's speed tracking and response to torque disturbance are excellent.

Further detailed discussion of the dynamic performance of the drive will not be presented here since it is not within the scope this thesis. It should also be noted that the purpose of the material presented in this chapter in regard to the field oriented control of induction motor drives is only to provide the theoretical basis for the next Chapter and therefore not an exhaustive treatment of the subject.

4 Coupled Simulation

The *dq-axes* model of the induction motor used in the simulation of the field oriented controlled drive system in chapter 3 assumes a sinusoidal air gap flux density distribution, although, in reality, this is not the case as the slot openings and magnetic saturation in the rotor and stator teeth produce considerable air gap flux density space harmonics [42]. In addition, this type of model does not take into account the influence of the magnetic nonlinearity of laminations, the slip frequency, and the operating temperature on motor parameters.

On the other hand, the finite element model of the induction motor (chapter 2) can depict the nature of the air gap flux distribution in the machine taking into account the factors described above with suitable accuracy. Also, in contrast to the *dq-axes* model, the FEM model takes into account the effects of material properties, motor geometry, and other operating conditions on motor parameters.

It is apparent from the above brief comparison that for accurate and realistic analysis of induction motors as well as the drive systems they are usually part of, the field model of the motor should be integrated with the converter and control circuit models. This is achieved in this chapter, by coupling <code>MagNet's</code> two-dimensional finite element model of the induction motor (chapter 2) with the <code>Matlab/Simulink</code> model of the field oriented controlled drive system (chapter 3).

The chapter starts out by discussing approaches for coupling the field model of induction motors with the external circuits of the power converter and the control system. Following that, the coupling mechanism implemented in this thesis is illustrated. Finally, the FOC induction motor drive system is simulated using this approach and the results are presented.

4.1 Coupling methods

The methods used for coupling the field computation of the induction motor with the transient simulation of the drive system that the motor is part of, can be classified into two general groups; the direct and indirect coupling methods. The classification is based on the approach taken to couple the field equations of the motor with the external circuit equations that represent the electrical sources and components connected to the motor windings.

4.1.1 Direct coupling

In this method, the finite element field equations, the external circuit equations, and the motion equations are assembled into a global system of equations and solved simultaneously.

The equations necessary for this coupling are summarized below:

• Field equation (equation (2.13) re-written here for convenience)

$$\nabla \times \nu \nabla \times \mathbf{A} = -\sigma \nabla V - \sigma \frac{\partial \mathbf{A}}{\partial t}$$
 (4.1)

 <u>Current equation</u> for calculating the total current flowing in the conductors of the induction motor

$$I = \iint_{conductor} \left(-\sigma \nabla V - \sigma \frac{\partial \mathbf{A}}{\partial t} \right) dx \, dy \tag{4.2}$$

- <u>Circuit equations</u> These describe the coupling between the total conductor current and the voltage (current) source through an external resistance, R_{ext} , and an inductance, L_{ext} , which, in 2D-FEA, represent the end winding resistance and inductance, respectively.
 - When a coil, formed by connecting conductors in series, is connected to a voltage or current source, the circuit equation relating the components is

$$V_{coil} = \{d\}_{coil}^{T} \{V\}_{coil} + L_{ext} \frac{dI_c}{dt} + R_{ext}I_c$$
 (4.3)

where V_{coil} is the voltage applied to the external terminals of the coil, and d is ± 1 and represents the polarity of each conductor in the coil,

ii. When a set of coils connected in parallel is connected to a voltage or current source with internal resistance, R_s , and inductance, L_s , the circuit equations relating the components are

$$V_s = R_s \{1\}^T \{I\}_{coil} + L_s \{1\}^T \left\{\frac{dI}{dt}\right\}_{coil} + V_{coil}$$
 (4.4)

where $\{1\}$ is a column vector of 1 with a dimension equal to the number of coils connected in parallel, and

 V_s is the source voltage

Equations of motion

$$J\frac{d\omega_r}{dt} = T_e - T_L - \Omega\omega_r$$

$$\omega_r = \frac{d\theta_r}{dt}$$
(4.5)

where Ω , is the viscous friction, and

 θ_r , is the rotor position.

Equations (4.1), (4.2), and (4.3), are coupled by the voltage applied to the terminals of the induction motor, V; equations (4.2), (4.3), and (4.4) are coupled by the conductor currents, I; and, equations (4.1), (4.2), and (4.5), by the magnetic vector potential, \mathbf{A} . After discretization and linearization of the field, circuit, and motion equations, the resulting matrix equations are assembled into a global system of equations describing the entire problem. Since this process is not within the scope of this thesis, it will not be discussed any further. This and additional information on the derivation of the equations summarized above and the methods for solving them can be found in reference [38].

As can be seen from the above discussion, the direct method of coupling the field computations of the induction motor with the analysis of its circuit equations is mathematically strong, and thus more reliable. However, when the circuit models involved are huge and complex, direct coupling of all the equations is not a very practical approach because each different case requires programming of a completely new set of equations. Inclusion of closed-loop control in directly coupled system equations, although possible, will require enormous effort and the control scheme will have to be simple. In addition, since the transient finite element analysis

will have to be time stepped with the same time step used to simulate the power electronic circuit, the overall computational cost of the directly coupled simulation is very high.

4.1.2 Indirect coupling

In this method, the field, circuit, and motion equations of the induction motor drive system are sequentially solved using two or more separate programs. The coupling between these programs is achieved through parameters that are common to the equations being considered. These parameters are exchanged between the coupled programs at each major time-step of the transient analysis/simulation of the whole system. Compared to direct coupling, considerable computational speed gains can be made since the coupled programs can use different time discretizations. Other advantages of the indirect coupling of the field-circuit-motion analysis include generality of applications, the ability to use specialized interfaces, part libraries and simulation capabilities of different applications, and the flexibility to control the programs independently preserving the accuracy and speed of individual programs.

Depending on the parameters used, there are two different ways of indirectly coupling the field analysis with the circuit and control analysis programs. The most common mechanism uses sources as coupling coefficients [43]. In this approach, if the induction motor is fed from a voltage (or current) source, the field analysis program computes the current flowing through the phase windings (or the voltage across the phase windings) and the mechanical speed of the

rotor, and supplies these parameters to the program that simulates the external circuits and control system. The control system processes the current (or voltage) and speed fed back from the field computation and sends switching signals to the power electronic converter to supply the field model of the induction motor with the appropriate phase voltage (or current). A block diagram that shows the flow of this process is shown in Figure 4-1.

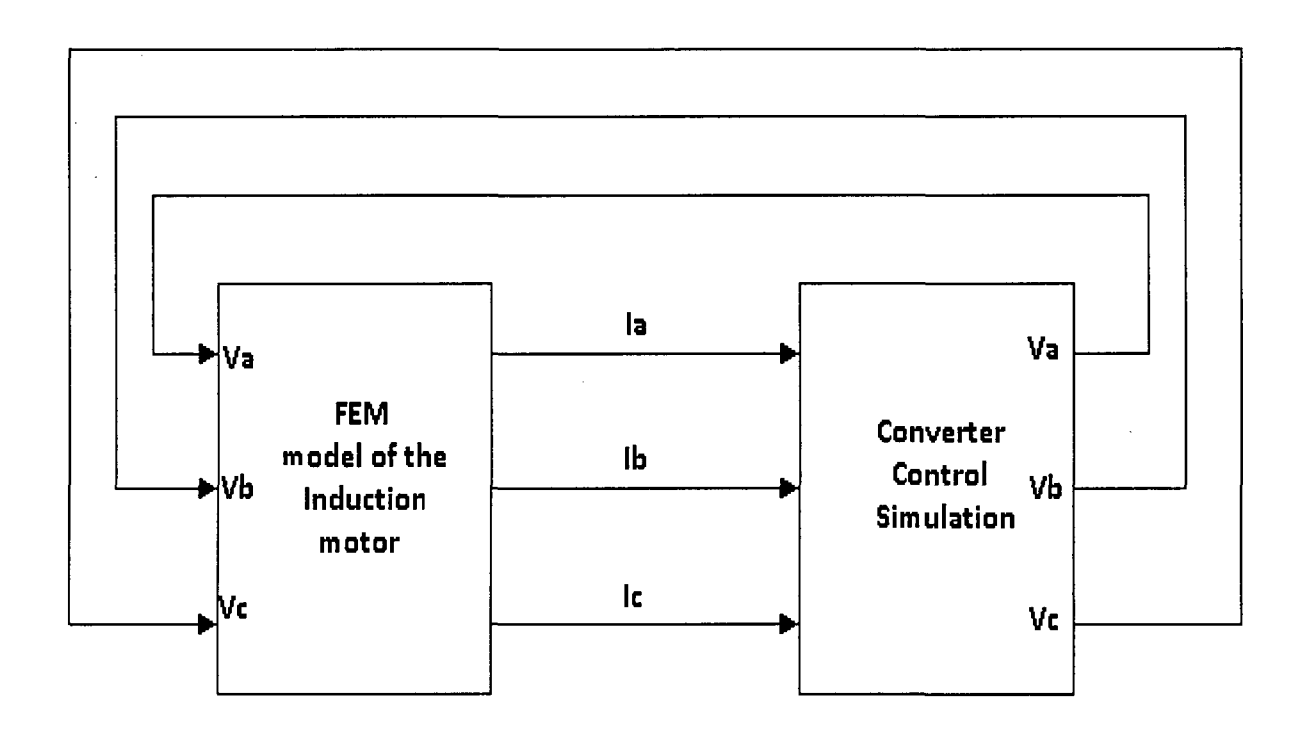


Figure 4-1 A block diagram of indirect coupling using sources

The alternative way of indirectly coupling the field and circuit analyses uses circuit parameters as coupling coefficients [44]. In this method, the induction motor is modeled by the electromotive force, e, and the dynamic inductance, L^{dyn} . The transient finite element analysis of the motor extracts and sends a parameter set consisting of the dynamic inductance matrix

and induced winding voltages, to the circuit and control simulation program at each of the FEA's time-steps. The control system determines the switching signals based on these coupling parameters and sends them to the power electronic converter to supply the field model of the induction motor with the appropriate phase voltage/current. A block diagram that shows the flow of this process is shown in Figure 4-2.

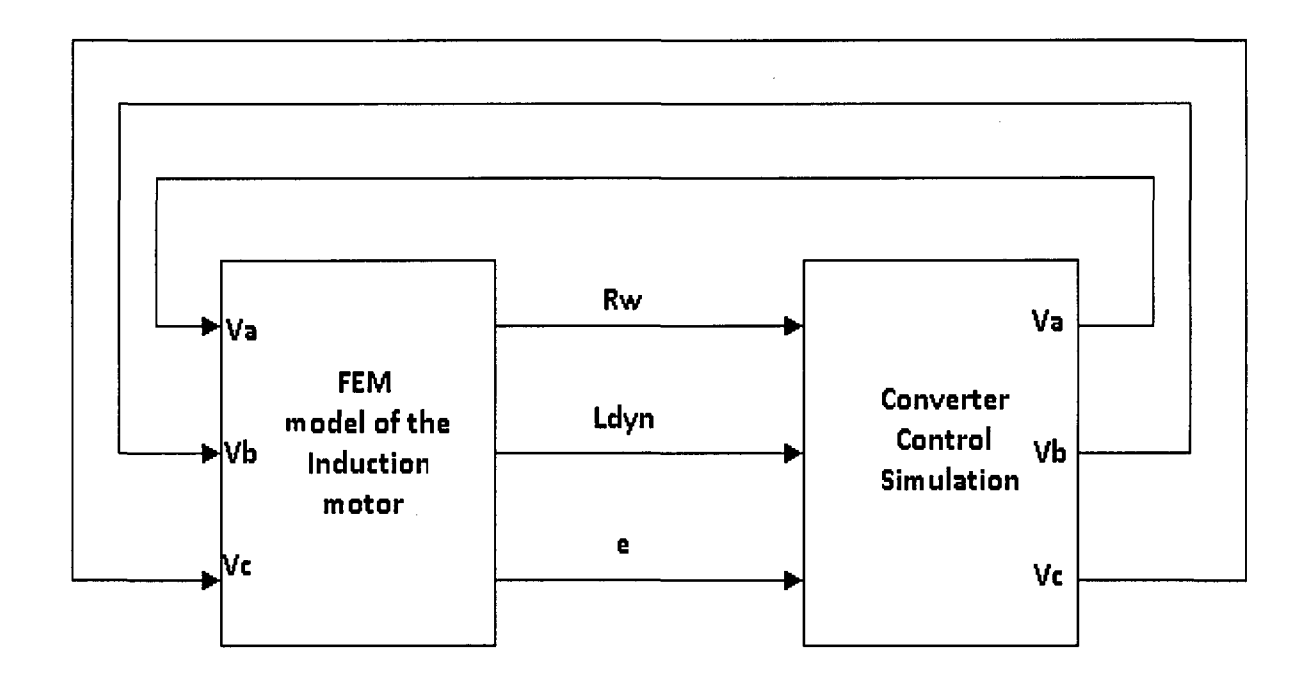


Figure 4-2 A block diagram of indirect coupling using $\,L^{dyn}$ and e

4.2 Implementation

In this thesis, the indirect method that uses sources as coupling parameters is adopted to couple the *Simulink* model of a field oriented controlled induction motor drive with *MagNet's*

field analysis of the motor. This approach is chosen because the output of the inverter model is an ideal voltage source and the flux and torque are calculated based on the stator current. The induction motor used here is the motor that was modeled and analyzed in chapter 2 and, whose *d-q* model is used in the FOC drive simulated in chapter 3. The same Simulink drive model of section 3.4 is used here, but the *d-q* model of the induction motor is replaced with the field model of the motor simulated in *MagNet*.

A plug-in provided by *MagNet* to link it with *Simulink* is used to facilitate the coupling between the two programs. This plug-in, shown in Figure 4-3, is a piece of software program that expands the capability of *MagNet* to work in conjunction with Simulink by providing the facility for data exchange between the two programs. There is an input-output pin pair on the plug-in for each voltage or current source defined in the *MagNet* model. The input and output pins corresponding to a voltage source are the source's voltage and current, respectively, and viceversa for a current source. Generally, voltage sources are preferred as they result in a more stable coupling for magnetic components and are less likely to yield non-physical conditions. An input-output pair is also provided by the plug-in for applying load torque and extracting the developed electromagnetic torque. There are two additional output pins for the motion component, corresponding to its position and speed.

The torque, voltage, current, speed, and position signals are transferred from *Simulink* to *MagNet* (and vice versa) during the coupled transient simulation of the drive. *MagNet* extracts the stator phase winding voltages of the motor from *Simulink's* transient simulation of the

converter and control system at each of its time-steps. After processing these inputs, MagNet provides Simulink with the stator winding currents and the mechanical speed of the rotor. These values are forced to be constant during MagNet's next time step, by the end of which time a new set of currents and speed will be available from MagNet. The Simulink time step used in the simulation of the converter and control system is $0.1 \, \mu s$. On the other hand, MagNet is set to run with a time step of $0.2 \, ms$. The selection of these time steps is based on finding an optimum between reasonable simulation time and adequate accuracy.

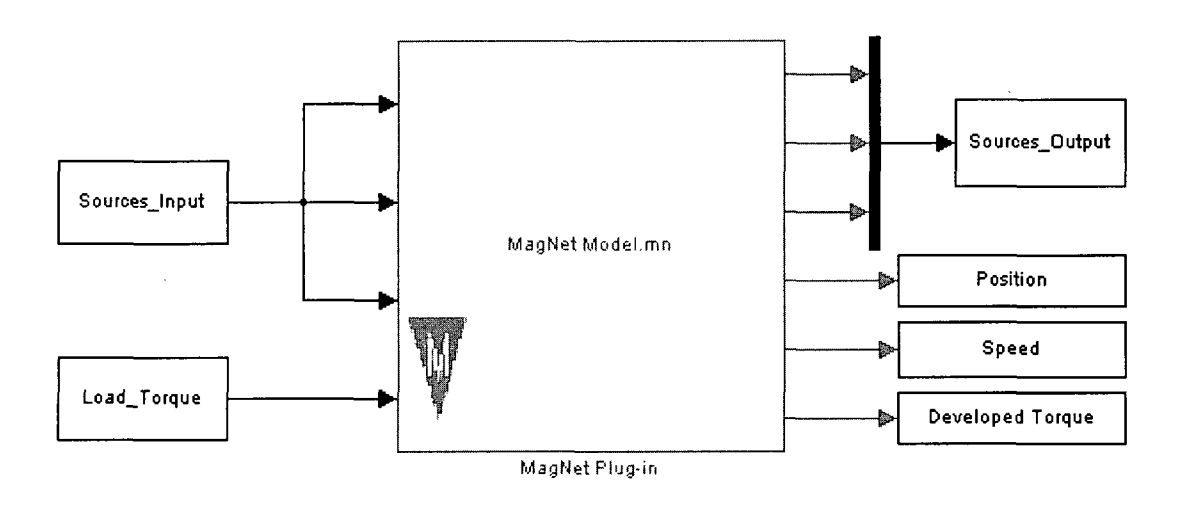


Figure 4-3 MagNet-Simulink Plug-in and its pins

The *Simulink* plug-in has a feature that permits *MagNet* to take advantage of symmetry, by allowing the currents and/or voltages to be scaled in the transfer between *Simulink* and *MagNet*. In this thesis case, since only a quarter of the induction motor is modeled in *MagNet*

and only a quarter of the stator coils are included as a result, the winding voltage is scaled by a factor of four in the *Simulink* component. As for the currents, since the windings of each phase in the modeled motor are connected in a series configuration, there is no need to scale them.

The schematic of the Simulink implementation of the coupled simulation for the indirect field oriented controlled induction drive is shown in Figure 4-4.

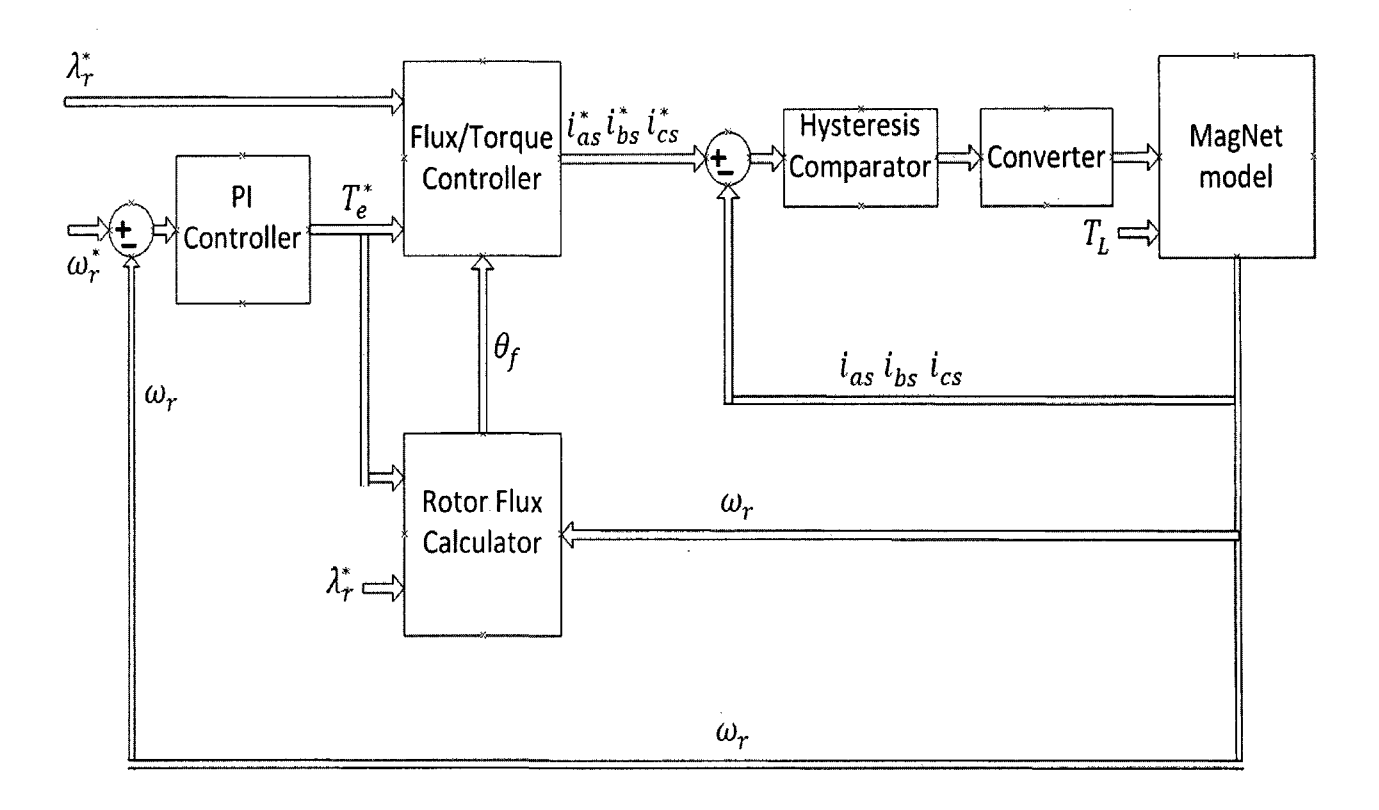


Figure 4-4 Schematic of the coupled simulation

4.3 Simulation results and discussion

The coupled simulation is tested under operating conditions that are similar to those used for testing the drive system simulated in chapter 3. These operating conditions are: a step change

in the speed reference and a step change in the load torque. In the first simulation, the motor is started with a speed reference of $120 \, rad/s$ and with no load. The motor speed, electromechanical torque, and stator currents observed during the starting of the induction motor drive are shown in Figure 4-5. In the second simulation, a load is applied to the motor while it is in steady state running at a speed of $120 \, rad/s$. The response of the induction motor drive to this load change is shown in Figure 4-6.

In this coupled simulation, *MagNet* takes the mechanical load on the motion component into account, as well as velocity effects such as the back *emf*. The resulting phase currents (shown in the second plots of Figure 4-5 and Figure 4-6) are calculated by performing a finite element analysis, and are returned to Simulink. The graphs shown below were generated by the scope blocks, which is just one of the many ways of extracting data from Simulink. Once the simulation is complete, *MagNet's* post-processor can also be invoked to plot the magnetic quantities, such as flux linkage and torque, as well as fields, such as flux density and current density.

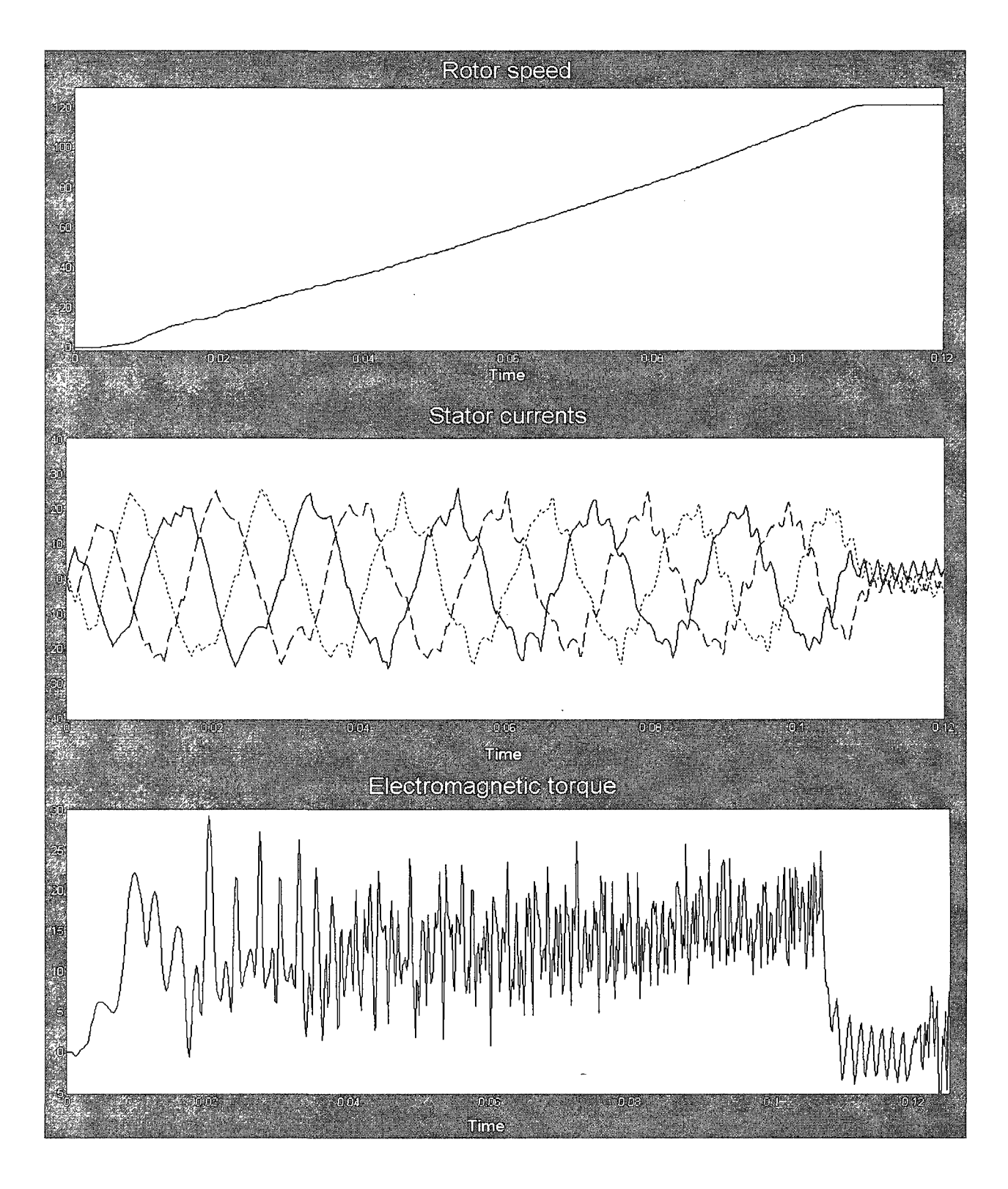


Figure 4-5 Coupled simulation waveforms of speed, current, and torque at start-up

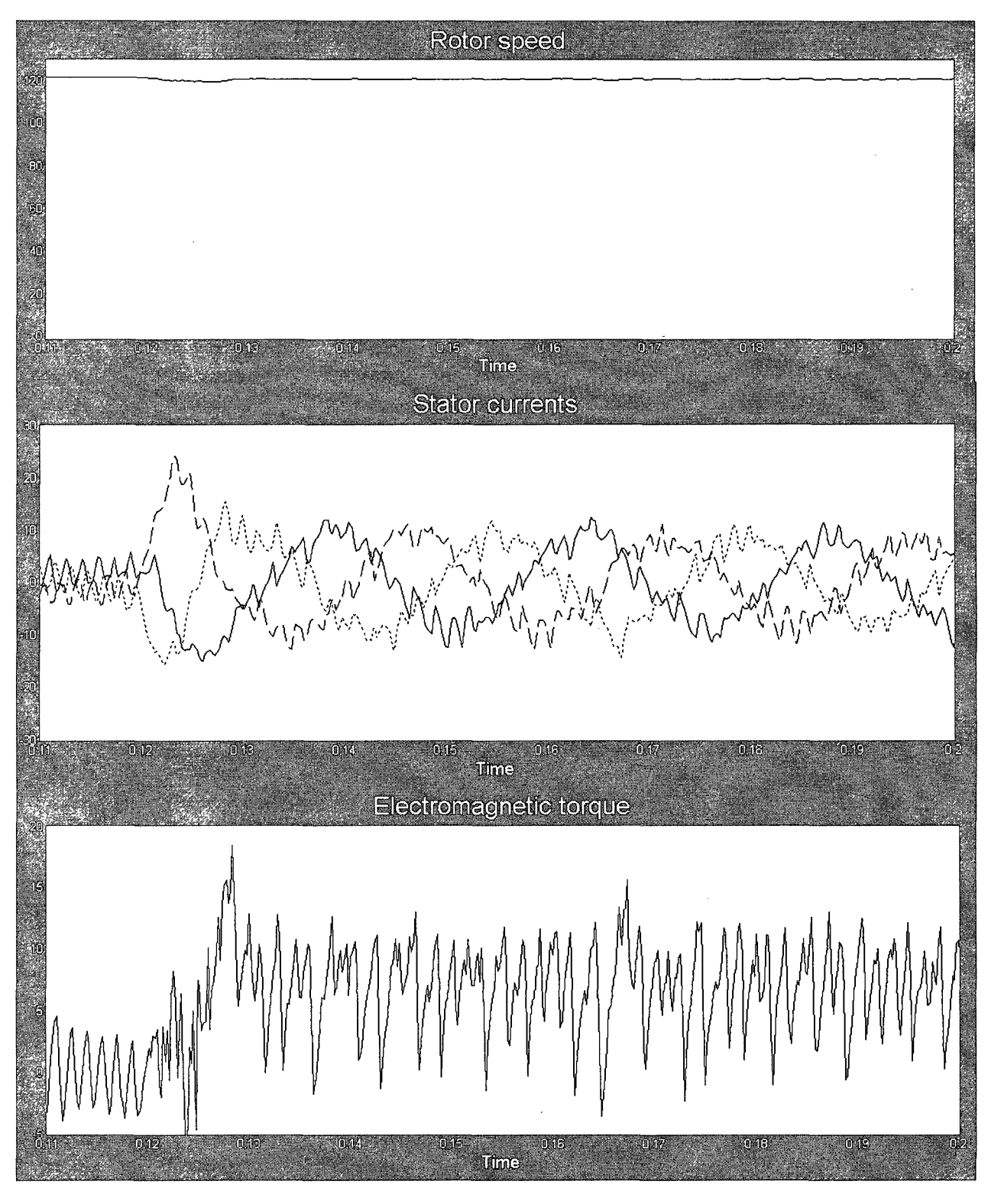


Figure 4-6 Coupled simulation waveforms of speed, current, and torque during load change

A summary of the simulation data is as follows.

- Simulation time: 0 to 200 ms (1000 MagNet time steps)
- Simulink time step: $0.1 \mu s$
- Total solve time: ≈7 hours.
- CPU: Intel Pentium IV running @ 2.8 GHz
- Polynomial order of elements in MagNet: 3
- Average number of elements in *MagNet*: 6500.
- Average number of unknowns in MagNet: 32000.

From the results of the simulations, it can be seen that the simulated drive system follows the speed and torque references given to it and that these responses are in good agreement with those found in chapter 3. From these observations, it can be concluded that the implemented coupled simulation is a practical approach for modeling and simulating indirect field oriented controlled induction motor drives.

5 Conclusion and Future Work

As mentioned in the literature review of this thesis, the concept of coupling the finite element model of an electromagnetic device with its associated converter and closed loop control models for accurate dynamic simulation of the whole system is not new. The purpose of this work is to extend this method to the modeling and simulation of indirect field oriented controlled induction motor drives as, to the best of the author's knowledge, this has not been reported so far in the literature. From the results obtained in chapter 4, it can be seen that this approach is promising. But, in order to make this coupled simulation more accurate and practical, additional work needs to be done.

5.1 Future work

In this section, future improvements that can be added to the system developed so far in this thesis are discussed.

5.1.1 Integration of thermal effects

As discussed in chapter 3, the performance of indirect field oriented control of induction motors depend strongly on accurate knowledge of machine parameters. Unfortunately, these parameters vary significantly during the operation of the motor due to factors such as operating temperature, magnetic saturation and skin effect. The variation in parameters

resulting from the electromagnetic state of the machine can be accounted for by using the electromagnetic field model of the machine. But in order to take into account parameter variations caused by the thermal state of the machine, the thermal model of the machine should also be coupled with the drive simulation along with the electromagnetic field model. Since both, the electromagnetic and thermal models are finite element based; incorporating the thermal analysis into the coupled simulation discussed in chapter 4 should not pose a lot of problems.

5.1.2 Comparison with measured results

In this thesis, the practicality of the implemented approach is studied by performing Simulink simulations of the drive system using the conventional method of modeling the induction motor (chapter 3) and coupling it with the transient finite element analysis of the induction motor (chapter 4). But, in order to conclusively verify the implemented approach, the results obtained in this thesis have to be compared with experimentally measured results. Therefore, one of the pieces of the future work in developing the proposed approach should be acquiring results from an experimental setup of the actual drive system and comparing them with the simulation results.

5.1.3 Response surface methodology

The high computational effort required to implement the proposed approach of simulation, may pose a challenge in integrating it into a routine design process. However, recent developments in multi-core architecture are opening the possibility of parallelizing coupled simulations in the near future. Until then, though, it may also be wise to investigate other possible methods of modeling that require less computational effort, but at the same time, like the field model discussed in chapter 2, dynamically take into account the effect of the electromagnetic state of the machine on its output parameters.

One promising approach that meets these requirements, but which requires further study of its ability to model the dynamic state of induction machines, is the response surface methodology (RSM) [45]. In this approach, a series of operating points of the motor, selected based on the design of experiments (DOE), are simulated using the FEM and the relationship between the inputs and the outputs of the motor at these points are plotted in a multi-dimensional space. The resulting hyper-surface is known as a response surface and shows the effects of the variations of each input on the output. Implicit in this relationship, i.e. between the input and output parameters of the motor, is also the effect of the electromagnetic state of the machine on the output parameters at each operating point.

Obviously, the computational effort that would be needed to simulate a drive system consisting of a motor modeled using RSM is a lot less than that is required by a simulation of the same drive system coupled with a full blown transient FEA. On the other hand, since FEA is used in

the process of determining the response surface model, the effect of the electromagnetic state of the machine on the output parameters will also be taken into account to some degree.

5.2 Summary

Chapter 1 started with a brief introduction and description of the problem considered in the thesis. Then previous works reported in the literature on the finite element analysis of induction motors, field oriented control scheme, and coupled simulations were reviewed. In chapter 2, a finite element analysis of an induction motor was performed using commercial electromagnetic simulation software. Motor parameters were extracted from the no-load and locked-rotor tests simulated in software. A transient analysis of the induction motor to simulate its start up condition was also performed and the results reported. A discussion of the two axes representation of the induction motor that is traditionally used in the dynamic simulation of induction motor drives started chapter 3. The principle of field orientation was presented followed by illustrations of the FOC drive systems, and the drive system was implemented in Simulink. The simulation results for different dynamic operations were reported. Chapter 4 brought together the information presented in chapters 2 and 3 to couple the magnetic field simulation of the induction motor with the dynamic simulation the FOC drive system. Available coupling methods for this purpose were explained and the implementation of the method chosen in this thesis elaborated on. The coupled simulation was tested using similar dynamic conditions to those simulated in chapter 3 and the results reported. Finally, this chapter

recommends possible future works that can make the coupled simulation implemented in this
thesis more reliable and practical.
83

References

- [1] Rahman, M.A., Chiba, A. and Fukao, T., "Super high speed electrical machines summary." *IEEE Power Engineering Society General Meeting*. 2004. Vol. 2, pp. 1272 1275.
- [2] Vas, P. and Drury, W., "Electrical machines and drives: present and future." 1996. 8th Mediterranean Electrotechnical Conference, . Vol. 1, pp. 67 74.
- [3] Chari, M.V.K. and Silvester, P., "Analysis of Turboalternator Magnetic Fields by Finite Elements." IEEE Transactions on Power Apparatus and Systems, 1971, Issue 2, Vols. PAS-90, pp. 454-464.
- [4] Chari, M. and Silverster, P., "Finite Element Analysis of Magnetically Saturated DC Machines." IEEE Transactions on Power Apparatus and Systems, 1971, Issue 5, Vols. PAS-90, pp. 2362 2372.
- [5] Ito, M., et al., "Analytical Model for Magnetic Field Analysis of Induction Motor Performance." IEEE Transactions on Power Apparatus and Systems, 1981, Issue 11, Vols. PAS-100, pp. 4582 4590.
- [6] Williamson, S. and Ralph, J. W., "Finite-element analysis of an induction motor fed from a constant-voltage source." IEE Proceedings, 1983, Issue 1, Vols. B-130, pp. 18-24.
- [7] Williamson and Bebb, M. C., "Analysis of cage induction motors A combined fields and circuits approach." IEEE Transactions on Magnetics, 1985, Issue 6, Vol. 21, pp. 2396 2399.
- [8] MacBain, J., "A Numerical Analysis of Time-Dependent Two-Dimensional Magnetic Fields." IEEE Transactions on Magnetics, 1981, Issue 6, Vol. 7, pp. 3259 3261.
- [9] Preston, T. W., Reece, A. B. J. and Sangha, P. S., "Induction Motor Analysis by Time-Stepping Techniques." IEEE Transactions on Magnetics, 1988, Issue 1, Vol. 24, pp. 471-474.
- [10] Arkkio, A., "Finite element analysis of cage induction motors fed by static frequency converters ." IEEE Transactions on Magnetics, 1990, Issue 2, Vol. 26, pp. 551-554.
- [11] Williamson, S. and Robinson, M.J., "Calculation of cage induction motor equivalent circuit parameters using finite elements." IEE Proceedings B: Electric Power Applications, 1991, Issue 5, Vol. 138, pp. 264-276.
- [12] Escarela-Perez, R. and Macdonald, D.C., "A novel finite-element transient computation of two-axis parameters of solid-rotor generators for use in power systems." IEEE Transactions on Energy Conversion , 1998, Issue 1, Vol. 13, pp. 49-54.

- [13] Mohammed, O.A., Liu, S. and Liu, Z., "A phase variable model of brushless dc motors based on finite element analysis and its coupling with external circuits." IEEE Transactions on Magnetics, 2005, Issue 5, Vol. 41, pp. 1576-1579.
- [14] Hasse, K., "Zum dynamischen Verhalten der Asynchronmaschine bei Betrieb mit variabler Ständerfrequenz und Ständerspannung." 1968, Vols. ETZ-A 89, pp. 387-391.
- [15] Blaschke, F., "The Principle of Field Orientation Applied to the New Transvector Closed-Loop Control System for Rotating Field Machines." *Siemens Review.* 1972, Vol. 39, pp. 217 220.
- [16] Gabriel, R. and Leonhard, W., "Field oriented control of a standard AC motor using microprocessors." IEEE Transactions on Industry Applications, 1980, Issue 2, Vols. IA-16, pp. 186-192.
- [17] Matsuo, T. and Lipo, T.A., "A rotor parameter identification scheme for vector controlled induction motor drives." IEEE Transactions on Industry Applications, 1985, Issue 3, Vols. IA-21, pp. 624-632.
- [18] Holtz, J. and Thimm, T., "Identification of the machine parameters in a vector-controlled induction motor drive." IEEE Transactions on Industry Applications, 1991, Issue 6, Vol. 27, pp. 1111-1118.
- [19] Yang, G. and Chin, T.-H., "Adaptive-speed identification scheme for a vector-controlled speed sensorless inverter-induction motor drive." IEEE Transactions on Industry, 1993, Issue 4, Vol. 29, pp. 820-825.
- [20] Lin, Faa-Jeng, Su, Ho-Ming and Chen, Hong-Pong., "Induction motor servo drive with adaptive rotor time-constant estimation." IEEE Transactions on Aerospace and Electronic Systems, 1998, Issue 1, Vol. 34, pp. 224-234.
- [21] Piriou, F. and Razek, A., "Coupling of Saturated Electromagnetic Systems to Non-Linear Power Electronic Devices." IEEE transactions on magnetics, 1987, Issue 1, Vol. 24, pp. 274-277.
- [22] Smith, A.C., Williamson, S. and Smith, J.R., "Transient currents and torques in wound-rotor induction motors using the finite-element method." IEE Proceedings B: Electric Power Applications , 1990, Issue 3, Vol. 137, pp. 160-173.
- [23] Meunier, G., Shen, D. and Coulomb, J.-L., "Modelisation of 2D and axisymmetric magnetodynamic domain by the finite elements method." IEEE Transactions on Magnetics, 1988, Issue 1, Vol. 24, pp. 166-169.
- [24] Demenko, A., "Equivalent RC networks with mutual capacitances for electromagnetic field simulation of electrical machine transients." IEEE Transactions on Magnetics, 1992, Issue 2, Vol. 28, pp. 1406-1409.

- [25] Chaudhry, S.R., Ahmed-Zaid, S. and Demerdash, N.A., "Coupled finite-element/state-space modeling of turbogenerators in the ABC frame of reference the short-circuit and load cases including saturated parameters." IEEE Transactions on Energy Conversion, 1995, Issue 1, Vol. 10, pp. 63-70.
- [26] Dular, P., Henrotte, F. and Legros, W., "A general and natural method to define circuit relations associated with magnetic vector potential formulations." IEEE Transactions on Magnetics, 1999, Issue 3 PART 1, Vol. 35, pp. 1630-1633.
- [27] Demenko, A., "Time-stepping FE analysis of electric motor drives with semiconductor converters." IEEE Transactions on Magnetics, 1994, Issue 5, Vol. 30, pp. 3264 3267.
- [28] Ito, M., et al., "Coupled magnetic field analysis with circuit and kinematics modelings of brushless motors." IEEE Transactions on Magnetics, 1997, Issue 2, Vol. 33, pp. 1702 1705.
- [29] Ho, S.L., et al., "Performance analysis of brushless DC motors including features of the control loop in the finite element modeling." IEEE Transactions on Magnetics, 2001, Issue 5, Vol. 37, pp. 3370 3374.
- [30] Jabbar, M.A., Phyu, Hla Nu and Liu, Z.J., "Analysis of the starting process of a disk drive spindle motor by time stepping finite element method." IEEE Transactions on Magnetics, 2004, Issue 4, Vol. 40, pp. 3204 3206.
- [31] Kuo-Peng, P., et al., "Analysis of a combined converter-electromagnetic device by taking into account its control loop." IEEE Transactions on Energy Conversion, 1999, Issue 4, Vol. 14, pp. 1430 1434
- [32] Roel Ortiz, J.L., et al., "Coupling static converter with control loop and non-linear electromagnetic devices." IEEE Transactions on Magnetics, 2001, Issue 5, Vol. 37, pp. 3514 3517.
- [33] Manot, G., et al., "Integration of control loops in coupled field circuit model to study magnetic devices supplied by power electronic converter and their control." COMPEL The International Journal for Computation and Mathematics in Electrical and Electronic Engineering, 2002, Issue 4, Vol. 21, pp. 563-572.
- [34] Kanerva, S., et al., "Recent Developments of Electrical Drives." Cracow, Poland: s.n., 2004. Proceedings of the 16th International Conference on Electrical Machines. pp. 83-92.
- [35] Infolytica Corporation., *Infolytica Corporation Web site*. [Online] MagNet 6.25, 2007. www.infolytica.ca.
- [36] Boldea, I. and Nasar, S. A., The Induction Machine Handbook. Boca Raton: CRC Press LLC, 2002.
- [37] Infolytica Corporation., MagNet Documentation. [Online] 2007. http://www.infolytica.ca/.
- [38] Salon, S.J., Finite element analysis of electrical machines. Troy: Kluwer Academic Publishers, 1995.

- [39] Wu, B., High power converters and AC drives. New Jersey: Wiley-IEEE Press, 2006.
- [40] Ho, E.Y.Y. and Sen, P.C., "Decoupling control of induction motor drives." IEEE Transactions on Industrial Electronics, 1988, Issue 2, Vol. 35, pp. 253-262.
- [41] Bose, B., Power Electronics and Motor Drives: Advances and Trends. s.l.: Elsevier Inc., 2006.
- [42] Mohammed, O. A., et al., "Electrical Machine Operational Modeling Utilizing Coupled Electromagnetic and Electric Drives Simulations." COMPEL, 2005, Issue 2, Vol. 24, pp. 495-508.
- [43] Kanerva, S., " Data transfer methodology between a FEM program and a system simulator." 2001. IEEE-ICEMS Fifth International Conference on Electrical Machines and Systems. Vol. 2, pp. 1121-1124.
- [44] Kanerva, S., Seman, S. and Arkkio, A., "Inductance model for coupling finite element analysis with circuit simulation." IEEE Transactions on Magnetics, 2005, Issue 5, Vol. 41, pp. 1620-1623.
- [45] Dyck, D., et al., "Response surface models of electromagnetic devices and their application to design." IEEE Transactions on Magnetics, 1999, Issue 3 PART 1, Vol. 35, pp. 1821-1824.

Appendix A

No-load simulation result

No-Load Test - Static Solution

Stator Current l _a	Flux Linkage λ _a	Magnetizing Inductance $L_{m\lambda} = \lambda_a/I_a$	Magnetic Energy W _m	Magnetizing Inductance $L_{mW} = (2/3) * W_m/l^2$
0.098927233	0.054630032	0.552224404	0.004146126	0.282435662
0.247318083	0.136575081	0.552224404	0.025913289	0.282435662
0.494636166	0.273148663	0.552221373	0.103652126	0.282432858
0.989272333	0.545906836	0.551826649	0.414050545	0.282052774
1.978544666	1.042646979	0.52697672	1.528058379	0.260229765
2.967816999	1.331369778	0.448602383	2.561665294	0.19389066
3.957089332	1.447974511	0.365919086	3.151668572	0.134183023
4.946361665	1.51992663	0.307281742	3.627389244	0.098839643
5.935633998	1.573967178	0.265172546	4.067597864	0.076968412
6.924906331	1.619572006	0.233876377	4.508061422	0.062671597
7.914178664	1.659496506	0.20968651	4.954000277	0.052729429
8.903450997	1.695118166	0.190388892	5.405467683	0.045459564
9.89272333	1.727190347	0.174592	5.862024376	0.039932328

Locked-rotor simulation result

Locked Rotor Test - Time Harmonic

Rotor Frequency	Magnetic Energy	Rotor Joule Losses	Torque - Maxwell Stress Tensor	Torque - Rotor Joule Losses	Rotor Equivalent Inductance	Rotor Equivalent Resistance	Leakage Inductance	Rotor Resistance
09	0.958023813	134.6971409	0.761521989	0.714590526	0.006517162	0.458153072	0.006592223	0.469159254
55	0.960850637	130.4176013	0.801603581	0.75478567	0.006536392	0.44359683	0.006611595	0.454285084
20	0.963677507	126.2638951	0.850509148	0.803820922	0.006555623	0.429468592	0.006630874	0.439847107
45	0.966498886	122.2805323	0.911494823	0.864957829	0.006574816	0.415919752	0.006649978	0.426000393
40	0.969322749	118.5156658	0.989469963	0.943117702	0.006594026	0.403114097	0.006668886	0.412912873
35	0.972188322	115.0202724	1.09216754	1.046059709	0.006613519	0.391225016	0.006687742	0.400762634
30	0.975202101	111.8455278	1.232459445	1.186717907	0.006634021	0.380426576	0.006707039	0.38972904
25	0.97862669	109.0410868	1.433476835	1.388354238	0.006657318	0.370887671	0.006728085	0.379987415
20	0.983140072	106.6501928	1.741294202	1.697390537	0.006688021	0.362755387	0.006754362	0.371693995
15	0.990780509	104.6993565	2.262590583	2.221789351	0.006739997	0.356119896	0.006796453	0.364957248
10	1.009781632	103.1596628	3.313927595	3.283674053	0.006869256	0.350882848	0.006897152	0.35974026
IJ.	1.105352554	101.6377096	6.445895987	6.470457554	0.007519397	0.345706142	0.007394804	0.355171766
~	3.65081976	86.74219061	27.19658137	27.61089682	0.024835483	0.295041163	0.021457054	0.320939162

Appendix B

The Finite Element Method

The two most popular methods of deriving the finite element equations are the variational approach and the Galerkin approach. The later is a special case of the method of weighted residual (MWR). The variational method was the first applied to problems in magnetics and occupies a large part of the early literature. However, there are a number of practical cases in machinery analysis in which the variational expression either is not known or does not exist and where the weighted residual method can be applied. Due to the greater generality of the Galerkin approach, this method has increased in popularity and is used by most FEA tools, including *MagNet*.

The method of weighted residual is applied as follows. It starts with an operator equation

$$\mathcal{L}(x) = 0 \tag{A.1}$$

on region Ω with boundary condition on the boundary C. Then an approximate solution \hat{x} is substituted into the equation. Since $x \neq \hat{x}$, this results in a residual.

$$\mathcal{L}(\hat{x}) = R \tag{A.2}$$

The MWR now requires that the integral of the projection of the residual on a specified weighting function is zero over the domain of interest. The choice of the weighting function determines the type of MWR. As an example we take the time harmonic form of the diffusion

equation with A, the z component of the magnetic vector potential, as the unknown. For a linear two dimensional Cartesian problem,

$$\frac{1}{\mu}\frac{\partial^2 A}{\partial x^2} + \frac{1}{\mu}\frac{\partial^2 A}{\partial y^2} = -J_o + j\omega\sigma A \tag{A.3}$$

Where μ is the magnetic permeability, ω is the angular frequency, σ is the electrical conductivity, and J_0 is the applied current density.

Substituting an approximation, \hat{A} , for A gives a residual R.

$$R = \frac{1}{\mu} \frac{\partial^2 \hat{A}}{\partial x^2} + \frac{1}{\mu} \frac{\partial^2 \hat{A}}{\partial y^2} - j\omega \sigma \hat{A} + J_o$$
 (A.4)

Multiplying by a weighting function and setting the integral to zero

$$\int_{\Omega} RW dx \, dy = 0 \tag{A.5}$$

Substituting for *R*

$$-\iint_{\Omega} \left(\frac{1}{\mu} \frac{\partial^2 \hat{A}}{\partial x^2} + \frac{1}{\mu} \frac{\partial^2 \hat{A}}{\partial y^2} \right) dx \, dy + j\omega\sigma \iint_{\Omega} W \hat{A} \, dx \, dy = \iint_{\Omega} W J_o \, dx \, dy \tag{A.6}$$

Integrating the first term by parts,

$$\iint_{\Omega} W \left(\frac{1}{\mu} \frac{\partial^{2} \hat{A}}{\partial x^{2}} + \frac{1}{\mu} \frac{\partial^{2} \hat{A}}{\partial y^{2}} \right) dx \, dy =$$

$$j\omega\sigma \iint_{\Omega} \left(\frac{\partial W}{\partial x} \frac{\partial \hat{A}}{\partial x} + \frac{\partial W}{\partial y} \frac{\partial \hat{A}}{\partial y} \right) dx \, dy - \oint_{C} \frac{1}{\mu} W \frac{\partial \hat{A}}{\partial \hat{n}} dc$$
(A.7)

where the last term is on the boundary C with \hat{n} being the outward normal unit vector.

Next, this result is substituted into equation (A.6) and the surface integrals are broken into summations over small areas. To do this, the surface is meshed with triangles (finite elements) and the integral over the entire domain is replaced with the summation of the integral over the individual triangles.

$$\sum_{M} \left\{ \frac{1}{\mu^{e}} \iint_{\Omega_{e}} \frac{\partial W^{e}}{\partial x} \frac{\partial A^{e}}{\partial x} + \frac{\partial W^{e}}{\partial y} \frac{\partial A^{e}}{\partial y} \right\} dx \, dy + j\omega \sigma^{e} \iint_{\Omega_{e}} W^{e} A^{e} \, dx \, dy$$

$$- \frac{1}{\mu^{e}} \frac{\partial A}{\partial \hat{n}} \int_{C} W^{e} \, dc = J_{o} \iint_{\Omega_{e}} W^{e} \, dx \, dy$$
(A.8)

where M is the number of triangular elements.

Consider a triangular element (ijk) depicted in Figure (A.1). The vertices are nodes at which the unknown vector potential will eventually be calculated.

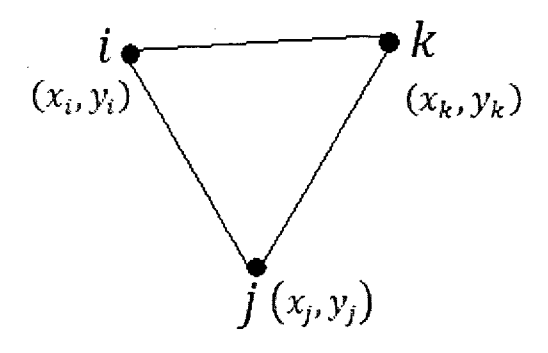


Figure A.1 First order element

If the potential in the element is assumed to vary linearly, the element is referred as a linear or first order element. With this approximation, the vector potential at any point in the triangle is expressed as

$$\hat{A} = C_1 + C_2 x + C_3 y \tag{A.9}$$

where C_1 , C_2 , and C_3 are constants to be determined. Since the vector potential varies linearly, the flux density, which is the derivative of the potential, is constant in the triangle.

At vertex , $x=x_i$, and $y=y_i$. At this point \hat{A} must be equal to \hat{A}_i , so that

$$C_1 + C_2 x_i + C_3 y_i = \hat{A}_i \tag{A.10}$$

Similarly for nodes j and k we have

$$C_1 + C_2 x_j + C_3 y_j = \hat{A}_j \tag{A.11}$$

and

$$C_1 + C_2 x_k + C_3 y_k = \hat{A}_k \tag{A.12}$$

This gives three equations and three unknowns. Next C_1 , C_2 , and C_3 are solved in terms of the potential and geometry. Using Kramer's rule

$$C_{1} = \frac{\hat{A}_{i} \begin{vmatrix} x_{j} & y_{j} \\ x_{k} & y_{k} \end{vmatrix} + \hat{A}_{j} \begin{vmatrix} x_{k} & y_{k} \\ x_{i} & y_{i} \end{vmatrix} + \hat{A}_{k} \begin{vmatrix} x_{j} & y_{i} \\ x_{j} & y_{j} \end{vmatrix}}{2\Delta}$$
(A.13)

Similarly

$$C_2 = \frac{\hat{A}_i \begin{vmatrix} 1 & y_k \\ 1 & y_j \end{vmatrix} + \hat{A}_j \begin{vmatrix} 1 & y_i \\ 1 & y_k \end{vmatrix} + \hat{A}_k \begin{vmatrix} 1 & y_j \\ 1 & y_i \end{vmatrix}}{2\Delta} \tag{A.14}$$

and

$$C_{3} = \frac{\hat{A}_{i} \begin{vmatrix} 1 & x_{j} \\ 1 & x_{k} \end{vmatrix} + \hat{A}_{j} \begin{vmatrix} 1 & x_{k} \\ 1 & x_{i} \end{vmatrix} + \hat{A}_{k} \begin{vmatrix} 1 & x_{j} \\ 1 & x_{j} \end{vmatrix}}{2\Delta}$$
(A.15)

where Δ is the area of the triangle.

Using these results \hat{A} can be expressed as

$$\hat{A} = \frac{(a_i + b_i x + c_i y)\hat{A}_i + (a_j + b_j x + c_j y)\hat{A}_j + (a_k + b_k x + c_k y)\hat{A}_k}{2\Delta}$$
(A.16)

where

$$a_i = x_j y_k - x_k y_j$$

$$b_i = y_j - y_k$$

$$c_i = x_k - x_j$$
(A.17)

The coefficients of the nodal potentials in equation (A.16) are called shape functions. The potential can be expressed as the sum of the shape functions times the nodal potential.

$$\hat{A} = \sum_{i=1}^{m} N_i(x, y) \hat{A}_i$$
 (A.18)

where there are m nodes in the element and N_i are the shape functions.

Writing the nodal potential in the element matrix form,

$$\hat{A}^e = \left(N_i^e, N_j^e, N_k^e\right) \begin{pmatrix} \hat{A}_i^e \\ \hat{A}_j^e \\ \hat{A}_k^e \end{pmatrix} \tag{A.19}$$

where

$$N_i^e = (a_i^e + b_i^e + c_i^e y)/2\Delta$$

 $N_j^e = (a_j^e + b_j^e + c_j^e y)/2\Delta$
 $N_k^e = (a_k^e + b_k^e + c_k^e y)/2\Delta$ (A.20)

In the Galerkin Method we chose the weighting function to be the same as the shape function.

$$W^e = \begin{pmatrix} N_i^e \\ N_j^e \\ N_k^e \end{pmatrix} \tag{A.21}$$

Taking derivative with respect to x and y,

$$\frac{\partial \hat{A}}{\partial x} = \frac{1}{2\Delta} (b_i^e, b_k^e, b_k^e) \begin{pmatrix} \hat{A}_i \\ \hat{A}_j \\ \hat{A}_k \end{pmatrix}$$

$$\frac{\partial \hat{A}}{\partial y} = \frac{1}{2\Delta} (c_i^e, c_k^e, c_k^e) \begin{pmatrix} \hat{A}_i \\ \hat{A}_j \\ \hat{A}_k \end{pmatrix} \tag{A.22}$$

and

$$\frac{\partial W^e}{\partial x} = \frac{1}{2\Delta} \begin{pmatrix} b_k^e \\ b_k^e \\ b_k^e \end{pmatrix}$$

$$\frac{\partial W^e}{\partial y} = \frac{1}{2\Delta} \begin{pmatrix} c_i^e \\ c_k^e \\ c_k^e \end{pmatrix} \tag{A.23}$$

Using these, the first term on the left side of equation (A.8) becomes

$$\frac{1}{\mu^{e}} \left(\frac{\partial W^{e}}{\partial x} \frac{\partial \hat{A}}{\partial x} + \frac{\partial W^{e}}{\partial y} \frac{\partial \hat{A}}{\partial y} \right) \iint_{\Omega_{e}} dx \, dy \tag{A.24}$$

It should be noted that

$$\iint dx \, dy = \Delta \tag{A.25}$$

Substituting

$$\frac{1}{\mu^{e}} \iint_{\Omega_{e}} \frac{\partial W^{e}}{\partial x} \frac{\partial \hat{A}^{e}}{\partial x} + \frac{\partial W^{e}}{\partial y} \frac{\partial \hat{A}^{e}}{\partial y} dx dy =$$

$$\frac{1}{4\mu^{e}\Delta} \begin{pmatrix} b_{i}^{2} + c_{i}^{2} & b_{i}b_{j} + c_{i}c_{j} & b_{i}b_{k} + c_{i}c_{k} \\ b_{i}b_{j} + c_{i}c_{j} & b_{j}^{2} + c_{j}^{2} & b_{j}b_{k} + c_{j}c_{k} \\ b_{i}b_{k} + c_{i}c_{k} & b_{j}b_{k} + c_{j}c_{k} & b_{k}^{2} + c_{k}^{2} \end{pmatrix} \begin{pmatrix} \hat{A}_{i} \\ \hat{A}_{j} \\ \hat{A}_{k} \end{pmatrix} \tag{A.26}$$

The coefficient matrix in equation (A.26) is sometimes referred as the stiffness matrix, S. The second integral in equation (A.8) becomes

$$j\omega\sigma^{e}\iint_{\Omega_{e}}W^{e}A^{e} dx dy = j\omega\sigma^{e}\iint_{\Omega_{e}} \binom{N_{i}^{e}}{N_{k}^{e}} (N_{i}^{e}N_{j}^{e}N_{k}^{e}) \begin{pmatrix} \hat{A}_{i} \\ \hat{A}_{j} \\ \hat{A}_{k} \end{pmatrix} dx dy$$

$$= \frac{j\omega\sigma^{e}\Delta}{12} \begin{pmatrix} 2 & 1 & 1 \\ 1 & 2 & 1 \\ 1 & 1 & 2 \end{pmatrix} \begin{pmatrix} \hat{A}_{i} \\ \hat{A}_{j} \\ \hat{A}_{k} \end{pmatrix}$$
(A.27)

This coefficient matrix is sometimes referred as the mass matrix, T.

The forcing function (right hand side of equation (A.8)) becomes

$$J_o \iint_{\Omega_e} \frac{(a_i + b_i x + c_i y)}{2\Delta} dx dy = J_o \frac{(a_i + b_i \overline{x} + c_i \overline{y})}{2}$$
(A.28)

where \bar{x} and \bar{y} are the coordinates of the centroid of the triangle.

Substituting the values found for a_i , b_i , and c_i (equation (A.17)) this becomes

$$\frac{a_i + b_i \bar{x} + c_i \bar{y}}{2} = \frac{\Delta}{3} \tag{A.29}$$

Assuming that J_0 is constant over the triangle,

$$J_o^e \iint_{\Omega_e} W^e \, dx \, dy = \frac{J_o^e \Delta}{3} {1 \choose 1} \tag{A.30}$$

Note |

In this Appendix, the derivation of the finite element equations from the time harmonic form of the diffusion equation is based on the assumption that the electromagnetic device is current. In the two dimensional vector formulation of Equation (A.3), J_o is obtained from the currents specified in the conducting regions. If the electromagnetic device is voltage driven, as it is the case in Chapter 4 of this thesis, the current is computed from the given voltage.